RESEARCH ARTICLE

AMERICAN JOURNAL OF BIOLOGICAL ANTHROPOLOGY
The Official Journal of the American Association of Biological Anthropologists

WILEY

The deep trabecular structure of first metacarpals in extant hominids

Christopher J. Dunmore[1] | Sebastian Bachmann[2] | Alexander Synek[2] | Dieter H. Pahr[2,3] | Matthew M. Skinner[1,4] | Tracy L. Kivell[1,4]

[1]Skeletal Biology Research Centre, School of Anthropology and Conservation, University of Kent, Canterbury, UK

[2]Institute of Lightweight Design and Structural Biomechanics, TU Wien, Vienna, Austria

[3]Department of Anatomy and Biomechanics, Division Biomechanics, Karl Landsteiner University of Health Sciences, Krems, Austria

[4]Centre for the Exploration of the Deep Human Journey, University of the Witwatersrand, Johannesburg, South Africa

Correspondence
Christopher J. Dunmore, Skeletal Biology Research Centre, School of Anthropology and Conservation, University of Kent, Canterbury, UK.
Email: c.j.dunmore@kent.ac.uk

Abstract

Objectives: Recent studies have associated subarticular trabecular bone distribution in the extant hominid first metacarpal (Mc1) with observed thumb use, to infer fossil hominin thumb use. Here, we analyze the entire Mc1 to test for interspecific differences in: (1) the absolute volume of trabecular volume fraction, (2) the distribution of the deeper trabecular network, and (3) the distribution of trabeculae in the medullary cavity, especially beneath the Mc1 disto-radial flange.

Materials and Methods: Trabecular bone was imaged using micro-computed tomography in a sample of *Homo sapiens* ($n = 11$), *Pan paniscus* ($n = 10$), *Pan troglodytes* ($n = 11$), *Gorilla gorilla* ($n = 10$) and *Pongo* sp., ($n = 7$). Using Canonical Holistic Morphometric Analysis (cHMA), we tested for interspecific differences in the trabecular bone volume fraction (BV/TV) and its relative distribution (rBV/TV) throughout the Mc1, including within the head, medullary cavity, and base.

Results: *P. paniscus* had the highest, and *H. sapiens* the lowest, BV/TV relative to other species. rBV/TV distribution statistically distinguished the radial concentrations and lack of medullary trabecular bone in the *H. sapiens* Mc1 from all other hominids. *H. sapiens* and, to a lesser extent, *G. gorilla* also had a significantly higher trabecular volume beneath the disto-radial flange relative to other hominids.

Discussion: These results are consistent with differences in observed thumb use in these species and may also reflect systemic differences in bone volume fraction. The trabecular bone extension into the medullary cavity and concentrations beneath the disto-radial flange may represent crucial biomechanical signals that will aid in the inference of fossil hominin thumb use.

KEYWORDS
cancellous bone, great apes, medullary cavity, pollex, thumb

1 | INTRODUCTION

Modern humans are unique among primates in using their hands primarily for manipulation and, due to obligate terrestrial bipedalism,

rarely for locomotion. It has been argued that this emancipation on the hominin hand allowed fossil hominins to become further specialized for manipulation (Richmond et al., 2016; Wood-Jones, 1917). The morphology of the modern human thumb is thought to facilitate our species' unique level of dexterity (Almécija, Smaers, & Jungers, 2015; Bardo et al., 2017; Kivell et al., 2016; Marzke, 2013; Napier, 1993) and our ability to habitually create, as well as use, complex technology (Key et al., 2019; Key & Dunmore, 2015; Marzke, 2013; Marzke et al., 1998; Marzke & Shackley, 1986; Rolian et al., 2011). A critical component of human dexterity is a forceful pad-to-pad precision grip in which the thumb is flexed, abducted and pronated toward the palmar pad of one or more fingers (Dunmore, Bardo, et al., 2020; Marzke & Wullstein, 1996; Napier, 1960). Non-human great apes have not yet been observed using pad-to-pad grips and are thought to not be capable of producing forceful precision grips due to their hand anatomy (Bardo et al., 2016, 2017; Christel, 1993; Neufuss et al., 2019; but see Marzke et al., 2015). Thus, the hard and soft tissue anatomy of the human thumb, including its long length relative to the length of the fingers, is thought to uniquely facilitate forceful pad-to-pad precision manipulation (Almécija, Smaers, & Jungers, 2015; Marzke, 1997, 2013). Identification of some or all of this modern human thumb anatomy in fossil hominins has been used to infer the manipulative and technological capabilities throughout human evolution (Alba et al., 2003; Almécija, Wallace, et al., 2015; Bowland et al., 2021; Dunmore, Skinner, et al., 2020; Galletta et al., 2019; Karakostis et al., 2021; Kivell et al., 2011; 2015; Maki & Trinkaus, 2011; Marchi et al., 2017; Marzke, 1997, 2013; Marzke et al., 2010; Morley et al., 2022; Napier, 1962; Niewoehner, 2006; Skinner et al., 2015a, 2015b; Susman, 1994; Tocheri et al., 2008; Trinkaus & Long, 1990). However, the functional significance of some of these features has been questioned (Almécija, Wallace, et al., 2015; Hamrick & Inouye, 1995; Shrewsbury et al., 2003; Williams-Hatala et al., 2016) and others occur in mosaic, often unique, combinations in some fossil hominins complicating the inference of thumb use (Kivell et al., 2011; Kivell et al., 2015).

The internal trabecular structure of bone can change in response to loads it experiences during life (Barak et al., 2011; Pontzer et al., 2006; Ruff et al., 2006) and offers a more direct link to bone function than external morphology alone. Though this process is mediated by genetic and ontogenetic factors (Lovejoy et al., 2003; Wallace et al., 2017), the concept of bone functional adaptation suggests that variation in the distribution of trabecular bone density reflects, at least in part, habitually loaded thumb joint positions in extant and fossil species (Dunmore, Bardo, et al., 2020; Dunmore, Skinner, et al., 2020; Kivell, 2016; Skinner et al., 2015a). However, to relate these thumb postures to specific grips, observations of hand use in extant species are necessary. A better understanding of how trabecular bone structure relates to observed hominid thumb use provides potential insight into loading during manipulative and locomotor hand grips, which can be often challenging to measure in endangered wild populations (Marzke et al., 2015; Neufuss, Humle, et al., 2017; Neufuss, Robbins, et al., 2017) or captive populations (Samuel et al., 2018; Wunderlich & Jungers, 2009). Understanding the

relationship (or lack thereof) between trabecular structure and habitual hand grips also provides additional comparative information to make more informed inferences of fossil hominin hand use where trabecular structure is preserved. Here, we analyze the entire trabecular structure in the extant hominid first metacarpal (Mc1), including within the base, medullary cavity and head, using a novel method that allows for holistic statistical comparisons between species throughout the entire bone (Bachmann et al., 2022).

Within the thumb, the human Mc1 is characterized by several features that are considered advantageous for forceful precision gripping. The articular surfaces of the human Mc1 differ from those of other extant hominids. The human distal articular surface is relatively flat and extended radio-palmarly, facilitating pronation of the metacarpophalangeal joint during precision gripping (Barmakian, 1992; Galletta et al., 2019). Similarly, the human Mc1 base is less curved, and radially extended relative to other hominids, facilitating abduction of the thumb at the carpometacarpal joint (Marchi et al., 2017; Marzke et al., 2010; Rafferty, 1990). Previous research has shown that, unlike other extant hominids, the distribution of trabecular bone beneath the human distal Mc1 joint is radially concentrated and that beneath the proximal joint it is radio-palmarly concentrated (Dunmore, Bardo, et al., 2020; Stephens et al., 2018). This distribution is consistent with a thumb habitually loaded in a forceful pad-to-pad grip (Dunmore, Bardo, et al., 2020). Together, this external and internal articular morphology is also thought to aid in the resistance of large forces transmitted through the thumb during manipulation (Galletta et al., 2019; Marzke et al., 2010; Rolian et al., 2011).

The shape of the human Mc1 diaphysis has also been argued to aid in the dissipation of large forces incurred by the human thumb during manipulation or tool-use, as it is more robust than in most other extant hominids (Hamrick & Inouye, 1995; Niewoehner, 2006; Rolian et al., 2011; Tocheri, Orr, Jacofsky, & Marzke, 2008b). The term robust, however, has been variously used to refer to the radio-ulnar width of the Mc1, the development of the distal epicondyles, the development of the entheses, or some combination of these (Bowland et al., 2021; Hamrick & Inouye, 1995; Morley et al., 2022; Susman, 1994). Overlap in the radio-ulnar width of the Mc1 between modern humans and gorillas, complicates our understanding of the potential manipulative or technological pressures that may have selected for it in human evolution (Bowland et al., 2021; Hamrick & Inouye, 1995; Morley et al., 2022; Susman, 1994). This radio-ulnar width of the Mc1 diaphysis is also highly dependent on the disto-radial flange (sometimes also referred to as a crest or ridge), which is a linear ridge of bone on the radial margin of the Mc1 diaphysis that is thought to provide greater surface area for the *m. opponens pollicis* (OP) insertion (Bowland et al., 2021; Karakostis et al., 2021; Maki & Trinkaus, 2011). This muscle is well-developed in modern humans and acts to flex and abduct the thumb, while it flexes and adducts the thumb in chimpanzees (Marzke et al., 1999). The projection of the human Mc1 disto-radial flange has also been modeled to provide an advantageous moment arm to this muscle, increasing biomechanical efficiency (Karakostis et al., 2021; Maki & Trinkaus, 2011). However, the actual insertion site of this muscle does not always completely

—WILEY—

conform to the disto-radial flange in humans (Trinkaus, 2016) as is implied by more common terms for this anatomical feature, such as "opponens pollicis crest". Moreover, the insertion site of this muscle is intraspecifically variable across extant hominids (Jacofsky, 2009; Karakostis & Lorenzo, 2016; van Leeuwen et al., 2018).

In humans, the OP insertion has been described as occurring across the entire radial margin of the human Mc1 diaphysis in cadavers (Jacofsky, 2009) and measured as restricted to the distal aspect of the disto-radial flange in an archeological population (Karakostis & Lorenzo, 2016). In chimpanzees, the OP insertion is described as occurring along the entire radial diaphysis of the Mc1 in one individual, but as more distally restricted and palmar in another (Jacofsky, 2009). Similarly, in bonobos, the OP insertion is on the radial aspect of the diaphysis, but in some individuals it extends further distally to the radial sesamoid (van Leeuwen et al., 2018). The OP insertion has been described as restricted to the proximal aspect of the radial margin of the diaphysis in two orangutans, but it is unclear how stable this location may be in a larger sample (Jacofsky, 2009). This intraspecific variability in extant hominid OP insertion sites implies that the etiology of the disto-radial flange is not solely driven by this muscle but does not imply that the OP has no effect on the disto-radial flange. The "enthesis organ concept" (Benjamin & McGonagle, 2009) holds that soft and hard tissues surrounding an insertion site also act to dissipate incurred loads and thus these tissues together form an "organ." The OP insertion sites that are not on the disto-radial flange might therefore still affect the size and shape of the flange to some extent. Thus, while the Mc1 disto-radial flange likely does develop in response to OP activity, as has been experimentally demonstrated for other flanges (Karakostis, Jeffery, & Harvati, 2019; Karakostis, Wallace, et al., 2019), the exact nature of this response is unclear (Bowland et al., 2021; Bucchi et al., 2020; Karakostis, Vlachodimitropoulos, et al., 2019; Williams-Hatala et al., 2016).

As trabecular bone can respond to forces experienced during life, analyzing this structure in the diaphyseal medullary cavity may help elucidate the relationship between OP forces, the disto-radial flange and thumb biomechanics in extant hominids. Indeed trabecular structure likely forms the internal part of the OP "entheseal organ" (Benjamin & McGonagle, 2009). Just as epiphyseal trabeculae are thought to transmit joint loads to diaphyseal cortical bone, medullary trabeculae likely transmit muscular forces to more proximal diaphyseal cortical bone (Currey, 2002; Martin et al., 2015b). Deeper trabeculae that receive loads from other parts of the trabecular network rather than purely from cortical bone, have been interpreted as reflective of functional signals in many other bones (Bird et al., 2021; Doershuk et al., 2019; Georgiou et al., 2020; Sorrentino et al., 2021; Tsegai et al., 2013; Zhou et al., 2014). Similarly, previous studies have revealed interesting interspecific variation in amount of trabecular bone within the Mc1 medullary cavity between humans and chimpanzees (Skinner et al., 2015a; Stephens et al., 2016) but these differences have not been quantitatively explored, due to methodological constraints, and it is unclear if this distribution is found in other extant hominids.

Here, we quantitatively analyze the distribution of trabecular structure in the entire Mc1, including within the base, medullary

cavity and head, of extant hominids for the first time, using a novel method that allows for holistic statistical comparisons between species throughout the entire bone (Bachmann et al., 2022). We test for: (1) interspecific differences in absolute trabecular bone volume fraction, (2) interspecific differences in the trabecular bone distribution extending beyond the subarticular region into the deeper trabecular network and (3) a trabecular bone concentration associated with the external disto-radial flange in the medullary cavity. We predict that: (1) the human Mc1 will have a significantly lower bone volume fraction than that of all other extant hominids as has been shown in other postcranial elements (Chirchir et al., 2015; Ryan & Shaw, 2015; Tsegai et al., 2018), (2) previously identified interspecific differences in subarticular distributions of trabecular bone (Dunmore, Bardo, et al., 2020; Dunmore, Skinner, et al., 2020) will extend deeper into the trabecular network as it functions to carry loads to the diaphysis (Currey, 2002; Martin et al., 2015b; Zhou et al., 2014), and (3) humans will have significantly more trabecular bone beneath the disto-radial flange than other extant hominids due to the insertion of a larger, more biomechanically efficient OP (Karakostis et al., 2021; Maki & Trinkaus, 2011; Marzke et al., 1999). The results will aid in the inference of thumb use and grips in fossil hominins.

2 | MATERIALS AND METHODS

2.1 | Sample

The complete trabecular network was analyzed in the Mc1 of *Homo sapiens* ($n = 11$), *Pan paniscus* ($n = 10$), *Pan troglodytes* ($n = 11$), *Gorilla gorilla* ($n = 10$), and *Pongo* sp. ($n = 7$). All specimens were complete and considered adult based on complete epiphyseal fusion of the Mc1 as well as other postcranial elements and free from signs of pathology. Human specimens were drawn from four populations: Nubians of ~5th century AD Sayala, Egypt (Paoli et al., 1993; Strouhal & Jungwirth, 1979, curated at the Natural History Museum, Vienna), Europeans from a cemetery in Inden, Germany (Grosskopf, 2015, curated at Georg-August-Universität Göttingen), 20th century individuals from Syracuse, Italy, and a Yámanas individual from 19th century Tiera del Fuego (Marangoni et al., 2011, both curated at the University of Florence). The permission to work on this material was sought from each curatorial institution and we adhered to all relevant guidelines. All non-human hominids were previously wild-caught. Each species sample was balanced for sex and overall sample size (Table 1). The human sample was drawn from right hands to avoid potential bias related to handedness (Faurie et al., 2005; see discussion).

2.2 | Image acquisition and segmentation

Specimens were scanned with a BIR ACTIS 225/300, Diondo D3, or a Skyscan 1172 high-resolution micro-CT scanner at the Department of Human Evolution, Max Planck Institute for Evolutionary Anthropology, Germany, or with the Nikon 225/XTH scanner at the Cambridge

TABLE 1 The study sample (*n* = 49), including taxonomic group, sex, and side

Side	Female	Male	Unknown	Total
Gorilla gorilla	**5**	**5**	**–**	**10**
Left	3	2	–	5
Right	2	3	–	5
Homo sapiens	**4**	**6**	**1**	**11**
Left	–	–	–	–
Right	4	6	1	11
Pan paniscus	**5**	**5**	**–**	**10**
Left	3	2	–	5
Right	2	3	–	5
Pongo sp.	**3**	**3**	**1**	**7**
Left	1	1	1	3
Right	2	2	–	4
Pan troglodytes	**5**	**6**	**–**	**11**
Left	2	3	–	5
Right	3	3	–	6
Sample total	**22**	**25**	**2**	**N = 49**

Note: Subtotals for each category are given in bold.

FIGURE 1 The canonical trabecular volume divided, into the head (orange), medullary cavity (cream), and base (green), in palmar, ulnar, dorsal and radial views (left to right). The dorso-radial epicondyle is marked with blue arrows. As mesh cells were not cut in these divisions, the edge of each segment is irregular.

Biotomography Centre, University of Cambridge, UK. Scans were performed at 100–160 kV and 100–140 μA using a brass or copper filter of 0.25–0.5 mm. The scans were reconstructed as volumetric images with an isometric voxel size of 24–41 μm depending on the size of the specimen and the scanner used. Access to these computed tomography (CT) scans is available via the relevant curatorial institution. Eight of the 49 volumetric images were digitally cleaned to remove minor sections of non-osseous adherent using the labels field functionality of Avizo 6.3 (Visualization Sciences Group). All images were then segmented into a binary phases of background and bone using the MIA-clustering algorithm, with a grid size of 15, 2 classes, and no probability filter (Dunmore et al., 2018).

2.3 | Trabecular bone analysis

Analysis of trabecular bone was conducted in Medtool 4.5 (Gross et al., 2014; Tsegai et al., 2013). In short, this method first identifies the periosteal and endosteal outline by shooting rays from the edge of an image until they contact cortical bone, and then another set of rays shoot from this periosteal edge until they contact the internal air of the dry bone. This endosteal edge is then closed, using a spherical kernel half the diameter of the measured average trabecular thickness in that bone, creating a trabecular volume (Pahr & Zysset, 2009). Trabecular thickness is measured using BoneJ for Image J (Doube et al., 2010; Hildebrand & Rüegsegger, 1997). Using the holistic morphometric analysis (HMA) of Medtool 4.5, this trabecular volume is then situated in a rectangular background grid and overlapping 5 mm volumes of interest, centred on each of the grid's 2.5 mm spaced
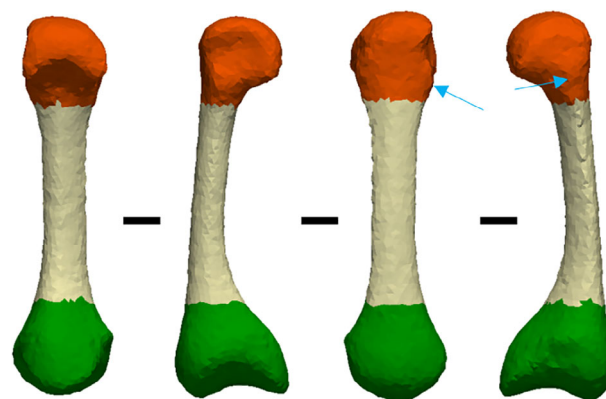
vertices, measure trabecular bone volume fraction (BV/TV). These values are then linearly interpolated onto a mesh of the trabecular volume. Left Mc1s were mirrored to ensure all specimens were in the same orientation before further processing.

Canonical holistic morphometric analysis (cHMA) was then used to quantitatively analyze the BV/TV values in the meshes of the Mc1 trabecular volumes at homologous points, which is described in detail by Bachmann et al. (2022). Briefly, this process uses a statistical free-form deformation model to create a canonical, or average, Mc1 trabecular volume shape. The canonical volume is then meshed and can then be morphed to each individual bone shape. HMA values, in this case BV/TV, can be measured in individual images and interpolated on the morphed mesh. The individual morphed meshes can then be morphed back to the canonical shape with individual HMA values mapped to homologous cells in the mesh, allowing for statistical analysis (Bachmann et al., 2022). To ensure the canonical volume accurately conformed to each individual morphed bone volume, mesh surface distances were compared. The average surface distances from individual morphed bone meshes to the canonical mesh were low (<0.3 mm), similar to those reported in a smaller sample by Bachmann et al. (2022), and surface distances were never more than 2.25 mm at any point. As this maximum surface distance is less than half the 5 mm diameter of the volumes of interest used to measure trabecular quantities, no part of the individual bones' trabecular structure was "missed" by the canonical volume, and so it was considered acceptable for further analysis (Figure S1).

The present analysis focuses on the distribution of BV/TV since it strongly correlates with biomechanical properties of bone (Stauber et al., 2006) and is not strongly affected by allometry (Barak et al., 2013; Doube et al., 2011; Ryan & Shaw, 2013). However, BV/TV has previously been argued to show systemic differences across extant hominids (Chirchir et al., 2015; Tsegai et al., 2018; but see Ryan & Shaw, 2015) and so relative measures have often been used to test for interspecific differences in distribution of BV/TV,

controlling for magnitude (Dunmore et al., 2019; Dunmore, Bardo, et al., 2020; Sukhdeo et al., 2020). Here we follow this approach and calculate relative BV/TV (rBV/TV) by dividing BV/TV at each mesh cell by the mean of all values for that individual Mc1. However, since the mean BV/TV value of the Mc1 is influenced by the inclusion of the medullary cavity, a volume with less trabecular bone than at the epiphyses, the canonical trabecular volume was subsequently divided into three segments (the head, medullary cavity, and base) for purpose of recalculating rBV/TV (Figure 1).

As the present study is focused on internal bone structure within the volume of the Mc1, rather than the external morphology as in previous studies (Bowland et al., 2021; Galletta et al., 2019; Morley et al., 2022), boundaries between each of the three segments were defined on the canonical trabecular volume created by cHMA to ensure geometrically homologous volumes required for analysis (Bachmann et al., 2022). The boundary between the medullary cavity and the head was defined as a plane orthogonal to the proximo-distal axis of the volume, where the edges of the trabecular volume are no longer convex in dorsal view and just beneath the most proximal aspect of the dorso-radial epicondyle on the canonical trabecular volume. The dorso-radial epicondyle, is the most proximal feature that has been used to measure hominid distal metacarpal shape (Galletta et al., 2019; Susman, 1979) and subarticular trabecular bone (Dunmore et al., 2019). The boundary between the medullary cavity and proximal base was more difficult to define as there are no readily identifiable homologous landmarks in this anatomical region. Therefore, this boundary was defined as a plane orthogonal to the proximo-distal axis of the volume at the point where the trabecular volume became substantially narrower in palmar view and more concave palmarly in ulnar or radial view, following the similar approach that previously adopted for the third metacarpal (Deckers et al., 2022). This approach yielded a boundary at approximately 23% of the overall length of the canonical trabecular volume and similar divisions to those previously used by Stephens et al. (2016) (Figure 1). The rBVTV values for each segment were recalculated using the mean BV/TV for each segment, allowing for the potential identification of subtler interspecific differences in segments of low BV/TV, such as the medullary cavity. The average BV/TV of each Mc1 segment was also statistically compared across species to test if any potential interspecific differences were driven by localized trabecular differences.

2.4 | Statistical analysis

The mean trabecular volume (BV/TV) of each specimen was calculated in each of the three segments outlined in Figure 1 and the whole Mc1 (Table S1). Interspecific differences were tested for in R using ANOVA and pairwise post-hoc Tukey's HSD tests (Table S2), as Levene's tests demonstrated no significant differences in homogeneity of variance between groups and Shapiro–Wilk tests showed no significant deviation from normality in any group, aside from one (Table S3). As the *H. sapiens* medullary cavity significantly deviated from normality, Kruskal-Wallis and post-hoc Dunn's tests with a

Bonferroni correction were run (Table S4). Significance was determined at $\alpha = 0.05$ for all tests.

To analyze the distribution of trabecular bone in each species, multivariate and mass-univariate approaches were employed. First, a principal components analysis (PCA) was run, treating each of the 10,848 tetrahedral elements of the canonical mesh as a variable. This summarized the species average pattern of rBV/TV distribution over the whole Mc1. Pairwise permutational MANOVAs were conducted on the first two principal components to test for interspecific differences in these patterns, rather than specific locations in the canonical trabecular bone volume. Further principal components did not consistently explain more variation than the neutral prediction of the Broken Stick method and so were not considered in the multivariate analysis (MacArthur, 1957; Figure S6). The assumption of multivariate homogeneity of group variances was tested for using ANOVA's on a euclidean distance matrix of the PC scores. This multivariate analysis was repeated for rBV/TV in each of the three segments.

Second, mass-univariate pairwise Kruskal-Wallis tests were conducted at homologous points throughout the canonical trabecular volume using cHMA (Bachmann et al., 2022). A version of this mass-univariate approach (Friston et al., 1994) has been employed in several recent studies (DeMars et al., 2021; Dunmore et al., 2019; Dunmore, Bardo, et al., 2020; Dunmore, Skinner, et al., 2020; Sorrentino et al., 2021) to identify the location of any significant differences in trabecular bone volume fraction between groups. Here, Type 1 error was controlled using a permutational approach, which has been demonstrated to be more sensitive and make less assumptions about the data than the Random Field Theory approach (Bachmann et al., 2022; Lazar, 2008; Nichols & Hayasaka, 2003). In brief, this method permutes the Mc1s between species to calculate a distribution of univariate test statistics for each mesh cell, to then be compared to the difference between observed species. The 95th percentile of the distribution of the maximum test statistic at any mesh cell in the Mc1 trabecular volume is then taken as the critical value for that set of pairwise interspecific comparisons, beyond which any mesh cell test statistic is deemed to demonstrate a significant difference between the observed species (Lazar, 2008). This approach was carried out using a custom python plugin for Medtool 4.5 and 20,000 permutations were run for each test. These tests were performed for rBV/TV over whole Mc1 and were also repeated for rBV/TV in each of the three segments.

3 | RESULTS

3.1 | Trabecular bone volume fraction in the first metacarpal

Mean BV/TV in the whole Mc1 was significantly higher in *P. paniscus*, and significantly lower in *H. sapiens* relative to all other species (Table 2, Figure 2). In the head segment, mean BV/TV was also significantly higher in *P. paniscus*, and significantly lower in *H. sapiens* relative to all other species. In the medullary cavity *H. sapiens* had

TABLE 2 Tukey HSD tests for interspecific differences in mean overall and segment BV/TV, over the whole Mc1 (white), the head (orange), the medullary cavity (cream) and the base (green)

	G. gor.	H. sap.	P. pan.	Pongo	P. trog.	G. gor.	H. sap.	P. pan	Pongo	P. trog.
G. gor.		**<0.001**	**0.006**	0.828	0.921		**<0.001**	0.160	0.825	>0.999
H. sap.	**<0.001**		<0.001	**0.018**	**<0.001**	**0.002**		**<0.001**	0.051	**<0.001**
P. pan.	**0.011**	**<0.001**		**<0.001**	**0.041**	**0.006**	**<0.001**		**0.023**	0.112
Pongo	0.930	**0.017**	**0.003**		0.373	0.874	0.087	**0.001**		0.866
P. trog.	0.999	**<0.001**	**0.004**	0.980		0.284	**<0.001**	0.419	0.059	
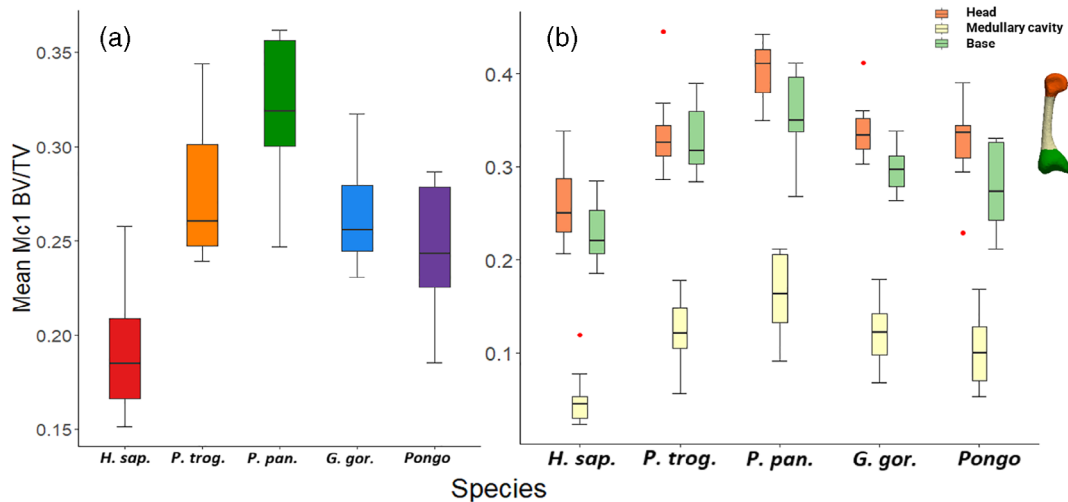
FIGURE 2 Mean overall Mc1 BV/TV by species (a), and per segment as colored in Figure 1 (b and inset). BV/TV is highest in the head, slightly lower in the base and lowest in the medullary cavity in all species.

significantly lower mean BV/TV compared to all other species except *Pongo*, where the difference approached significance ($p = 0.051$). *P. paniscus* had significantly higher mean BV/TV than *Pongo* in the medullary cavity. In the base, *H. sapiens* had significantly lower mean BV/TV than to all other species except *Pongo*, and *P. paniscus* had significantly higher mean BV/TV in comparison to *G. gorilla* and *Pongo*.

3.2 | Mean species trabecular bone distribution

The whole Mc1 of *H. sapiens* displayed a mean rBV/TV pattern concentrated in the radial region of the Mc1 head and radio-palmar region of the base (Figure 3a). These distribution patterns were clearer when rBV/TV was calculated from the respective segments alone (Figure 3b,d). *H. sapiens* also showed a concentration of rBV/TV in the disto-radial aspect of the medullary cavity when this segment is considered separately (Figure 3c). *P. paniscus*, *P. troglodytes*, and *Pongo* all showed a slight disto-ulnar concentration of rBV/TV in the Mc1 head and a lack of spatial differentiation of rBV/TV in the base (Figure 3a,b, d). *P. paniscus* and *P. troglodytes* had a concentration that extended further from the proximal epiphysis into the medullary cavity than in *Pongo*, *G. gorilla*, or *H. sapiens* (Figure 3a,c). *G. gorilla* demonstrated a more distinct ulnar concentration of rBV/TV in the head, and a slightly ulnar and strongly palmar concentration in the Mc1 base, as well as a

weak concentration of rBV/TV throughout the radial aspect of the medullary cavity (Figure 3).

3.3 | Volumetric multivariate analysis of trabecular bone distribution

A principal components analysis (PCA) of trabecular volume distribution in the whole Mc1 reduced the dataset to two principal components of interest for further analysis (Figure S6). Principal component 1 (PC1) explained over half (56%) of the variation in rBV/TV values at each mesh cell. The negative values on PC1 were driven by concentrations of rBV/TV throughout the Mc1 head, especially in the ulnar aspect, and a dorsal concentration of rBV/TV in the base that extended distally into the proximal medullary cavity. The positive values on PC1 were driven by concentrations of rBV/TV across most of the sub-articular surface of the Mc1 head, especially beneath the radio-palmar epicondyle, and a concentration beneath the radio-palmar region of the proximal sub-articular surface that extended disto-radially (Figure 4). PC2 accounted for 12.6% of the variation in rBV/TV values and was driven by more rBV/TV in the Mc1 head compared with the base at the positive extreme and a more balanced distribution between these regions at the negative extreme. Permutational pairwise MANOVAs found no significant difference

DUNMORE ET AL.

AMERICAN JOURNAL OF
BIOLOGICAL ANTHROPOLOGY
The Official Journal of the American Association of Biological Anthropologists

WILEY 7

FIGURE 3 The mean rBV/TV distribution of each species mapped to the canonical trabecular volume, as calculated from: the whole Mc1 in palmar view (a), head in palmar view (b), medullary cavity in radio-palmar view (c), and the base in proximal view (d). All cut models are within a translucent canonical mesh of cortical bone. A value of 1 represents a mesh cell with BV/TV equal to the average BV/TV of the rest of the mesh volume. D, distal; Do, dorsal; P, proximal; Pa, palmar; R, radial; U, ulnar
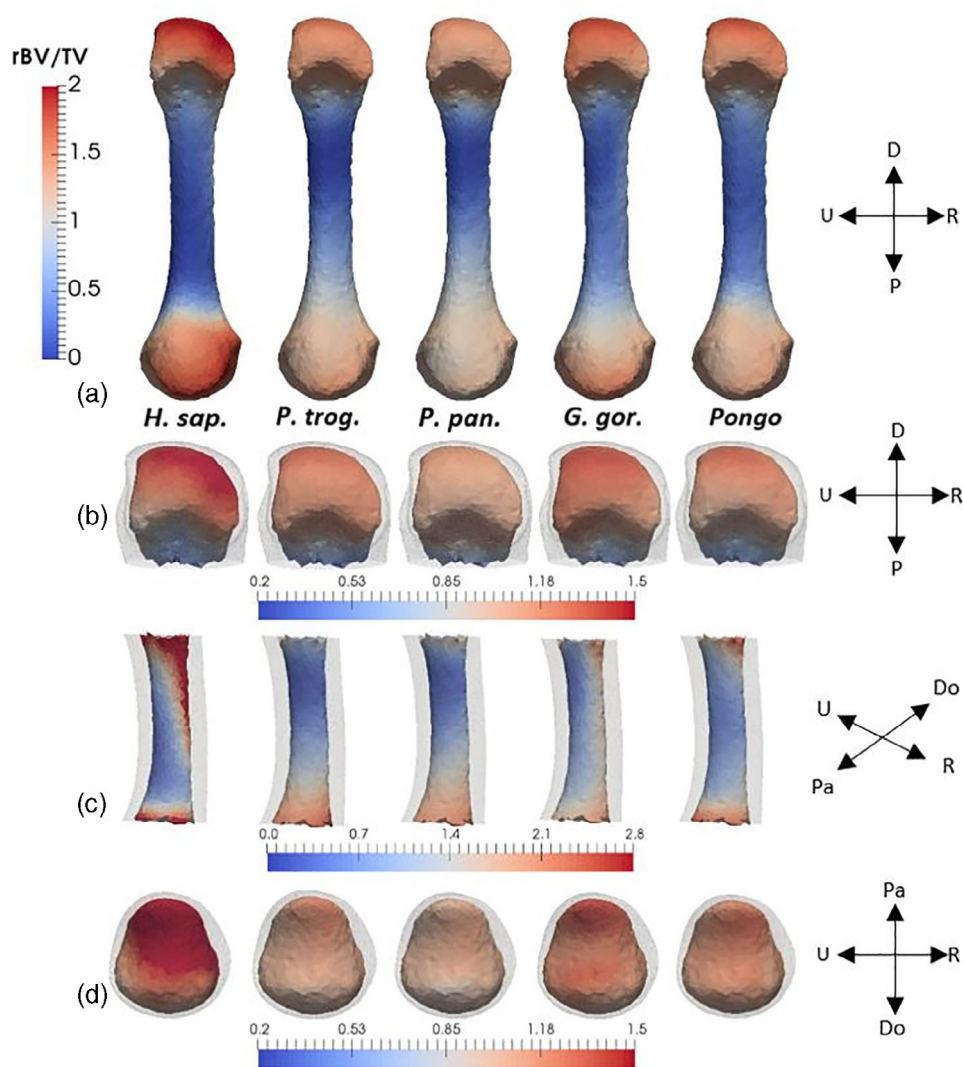

FIGURE 4 PCA of the rBV/TV patterns throughout the whole Mc1. Larger points denote the centroid of each species. The canonical trabecular volumes are colored by the signed loadings at two standard deviations (SD) of each principal component and thresholded at the 75th percentile of this range, to demonstrate volumetric trabecular structure. The volumes are within a translucent canonical mesh of cortical bone and given in palmar (left) and ulno-palmar (right) views.
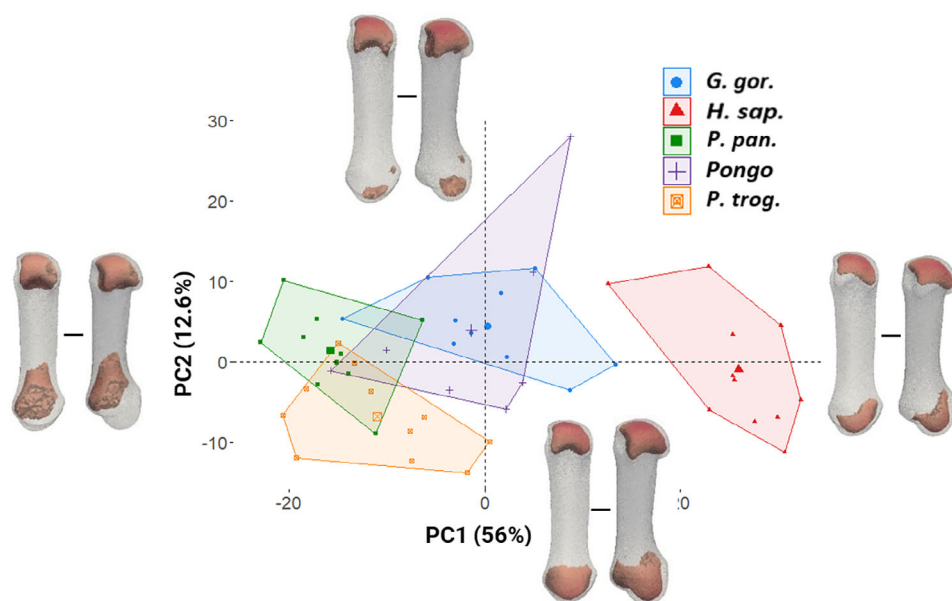
8 | WILEY—**BIOLOGICAL ANTHROPOLOGY**
AMERICAN JOURNAL OF
The Official Journal of the American Association of Biological Anthropologists

DUNMORE ET AL.

TABLE 3 Interspecific pairwise permutational MANOVAs on the first two principal components

	G. gor.	H. sap.	P. pan.	Pongo	P. trog.	G. gor.	H. sap.	P. pan	Pongo	P. trog.
G. gor.		<0.001	0.001	>0.999	<0.001		<0.001	<0.001	0.274	<0.001
H. sap.	0.001		<0.001	<0.001	0.000	<0.001		<0.001	0.004	<0.001
P. pan.	0.002	<0.001		0.011	0.050	<0.001	<0.001		0.017	>0.999
Pongo	>0.999	0.001	0.398		0.011	>0.999	<0.001	0.006		0.003
P. trog.	0.869	<0.001	0.008	0.555		0.014	<0.001	0.651	0.241	

Note: All omnibus tests were significant ($p < 0.001$) and only the base comparisons were subject to significant heterogeneity of variance ($p = 0.005$). However permutational MANOVAs are thought to be resistant to heterogeneity in multivariate variance in balanced designs (Anderson & Walsh, 2013) and univariate tests on PC1 yielded the same significant interspecific differences (Table S5).
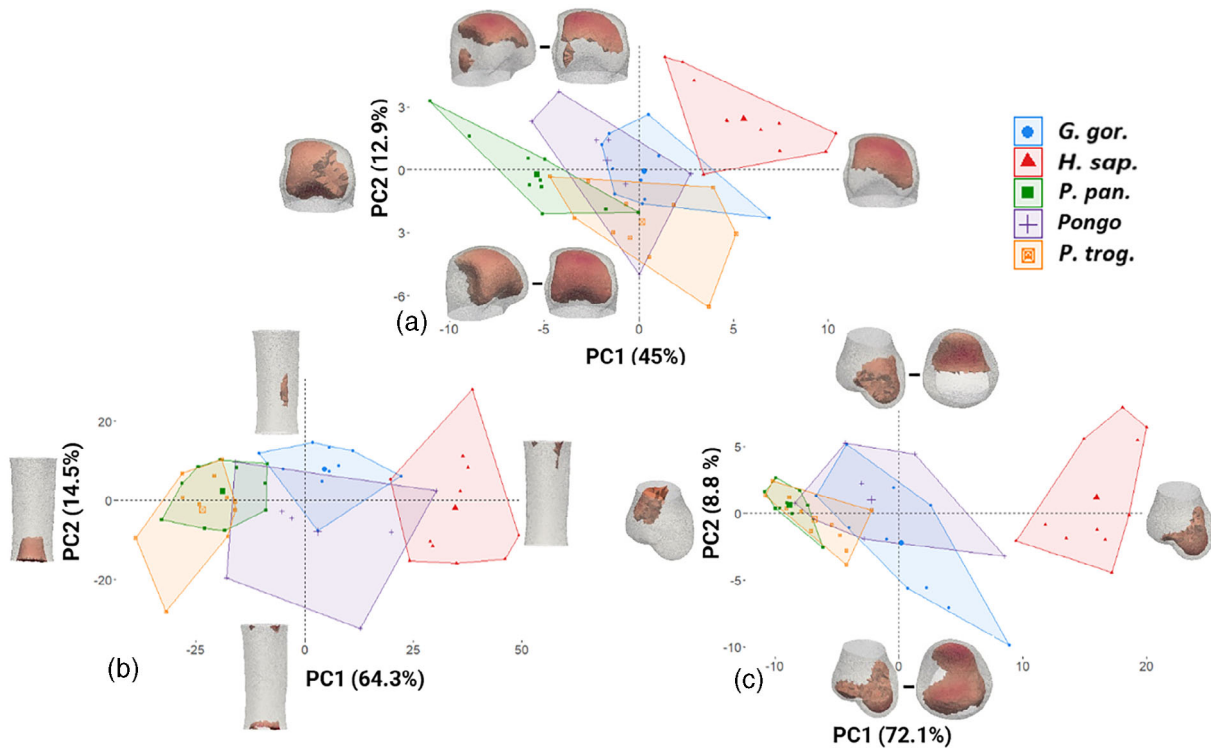

FIGURE 5 PCA of rBV/TV of the head in ulno-palmar and palmar view (a), medullary cavity in palmar view (b), and the base (c) in ulno-palmar (left) as well as proximal view (right). Larger points denote the centroid of each species. The canonical trabecular volumes are colored by the signed loadings at two SD of each principal component and thresholded at the 75th percentile of this range, to demonstrate volumetric trabecular structure. The volumes are within a translucent canonical cortical mesh.

between the rBV/TV distributions of *Pongo* and *Gorilla* and the difference between *Pan* species only approached significance. All other pairwise comparisons were significant, with *H. sapiens* demonstrating the largest interspecific differences (Table 3). These results reflect species positions on PC1, as PC2 did not separate species (Figure 4). PC2 was not solely driven by the *Pongo* outlier (Figure S2). The relative PC1 positions remained constant when species were split by sex, side and *H. sapiens* population (Figures S3–S5).

A separate PCA of rBV/TV within each of the three Mc1 segments revealed similar, but more accentuated, species patterns in rBV/TV distribution as the whole Mc1 analysis. PC1 of rBV/TV within the Mc1 head segment explained 45% of the variance. Positive PC1 values were driven by a concentration of sub-articular rBV/TV that

was skewed radially, especially in its palmar aspect. Negative PC1 values were driven by a rBV/TV concentration throughout the ulnar aspect of the Mc1 head segment. PC2 in this segment explained 12.9% of the variation and reflected a more distal and palmar concentration of rBV/TV at its positive and negative extremes, respectively (Figure 5a). Permutational pairwise MANOVAs demonstrated that *H. sapiens* was significantly different from all other species, and *P. paniscus* was significantly different from both *P. troglodytes* and *Gorilla* (Table 3).

In the PCA of rBV/TV in the medullary cavity, PC1 explained 64.3% of the variation. Negative PC1 values reflected a rBV/TV concentration in the proximal region of the medullary cavity while positive values reflected a primarily disto-radial concentration. PC2
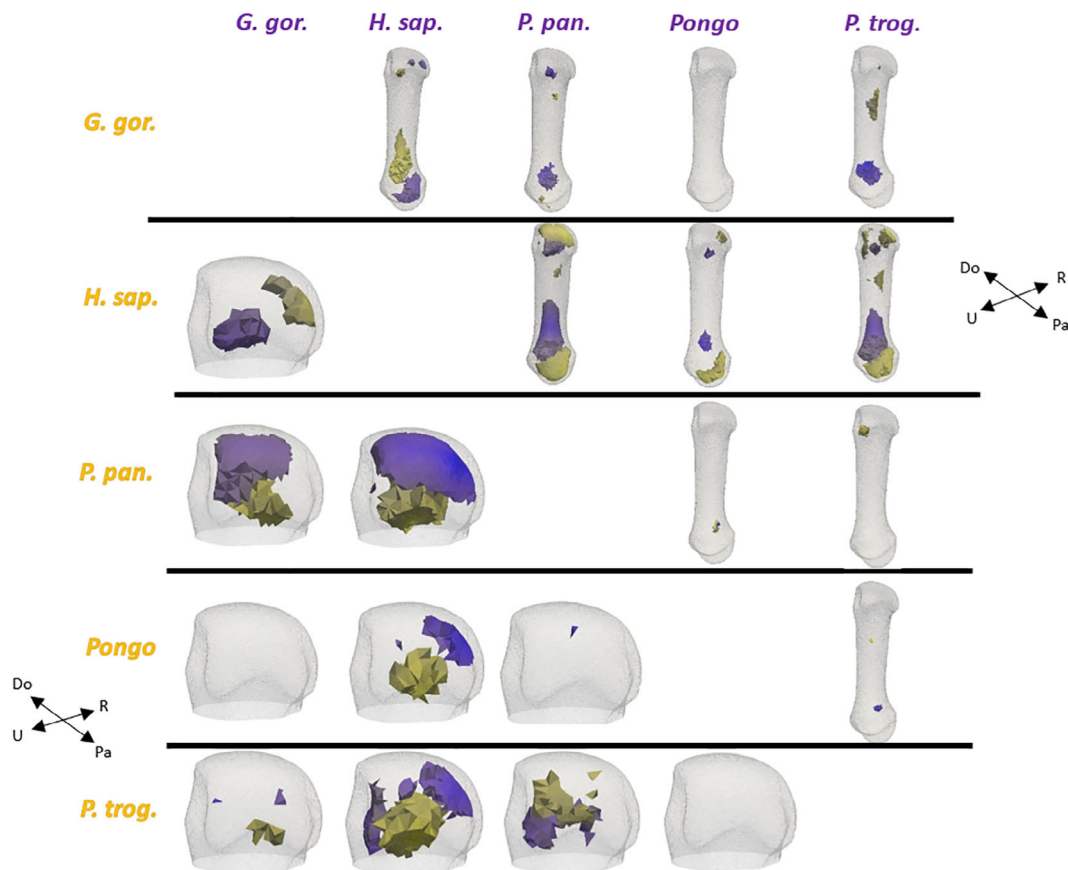
FIGURE 6 Significant interspecific differences in rBV/TV per cell in the whole Mc1 (top right) and Mc1 head (bottom left). The canonical trabecular volumes are thresholded at the critical value determined by the permutation control of type 1 error rate and colored by significantly higher rBV/TV in each species, as specified by the color of the row and column. The volumes are within a translucent canonical mesh of cortical bone. D, distal; Do, dorsal; P, proximal; Pa, palmar; R, radial; U, ulnar

explained 14.5% of the remaining variance, positive values reflected a rBV/TV concentration on the radial side of the medullary cavity, while the negative extreme reflected small concentrations of rBV/TV at the proximal and distal ends of the cavity segment (Figure 5b). Although this morphological variation was not highlighted in the whole Mc1 PCA (Figure 4), permutational pairwise MANOVAs of the medullary cavity rBV/TV again showed that *H. sapiens* were significantly different from all other species, and that both *Pan* species were significantly different from *Pongo* and *G. gorilla*, which were not significantly different from each other. However, the high range of variation in *Pongo* may drive a lack of significant differences with other species (Figure 5b, Table 3).

In the PCA of rBV/TV in the base, PC1 explained 72.1% of the variance. The negative extreme of PC1 was driven by a dorsal rBV/TV concentration that extended distally, while the positive extreme was driven by a subarticular radio-palmar concentration that extended disto-radially (Figure 5c). PC2 explained 8.8% of the remaining variance and its positive values were driven by a palmar concentration of rBV/TV. The negative values of PC2 were driven by a radially skewed diffuse sub-articular pattern of rBV/TV (Figure 5c). Permutational pairwise MANOVA's revealed *H. sapiens* was significantly different from all other species, *G. gorilla* was significantly different from both

Pan species, and *P. pansicus* was significantly different from *Pongo* (Table 3). The low range of variation in both *Pan* species should also be noted (Figure 5c) and likely drove the significantly different group variances ($F = 4.2959$, $p = 0.005$). As this is a violation of the assumption multivariate homogeneity of variances (but see Anderson & Walsh, 2013); unlike any other pairwise permutational MANOVA analysis presented here, these group comparisons were re-run only using PC1 scores. For univariate PC1 scores, all groups were normally distributed and did not violate the univariate assumption of homogeneity of variances. The pairwise comparisons yielded the exact same set of significant group differences as the multivariate analysis (Tables S5 and 3).

3.4 | Volumetric mass-univariate analysis of trabecular bone distribution

Localized differences in rBV/TV largely reflected multivariate patterns of trabecular distribution reported above. Specific regions of significant differences are depicted in color maps in Figures 6 and 7. Mass-univariate Kruskal-Wallis tests of the whole Mc1 reflected significantly more rBV/TV in the radial aspect of the head and in the radio-
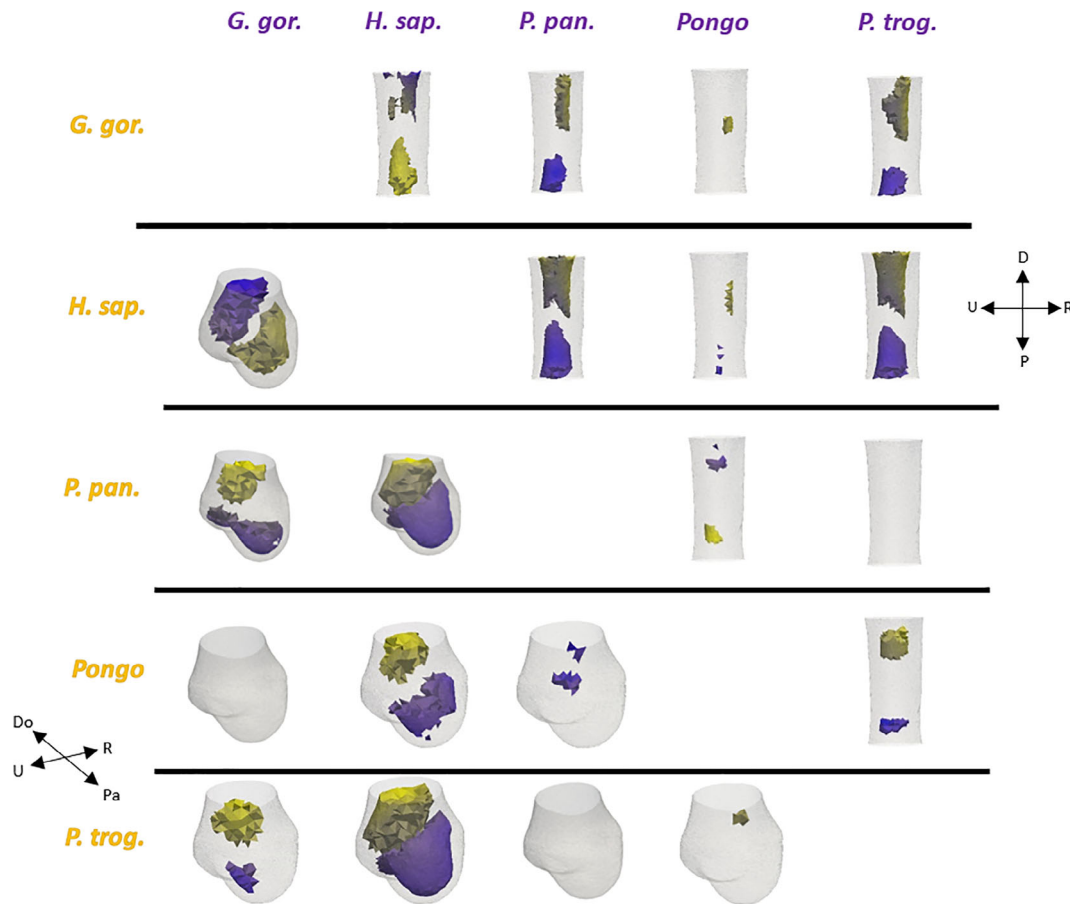
10 | WILEY—**AMERICAN JOURNAL OF BIOLOGICAL ANTHROPOLOGY**
The Official Journal of the American Association of Biological Anthropologists

DUNMORE ET AL.

FIGURE 7 Significant interspecific differences in rBV/TV per cell in the Mc1 medullary cavity (top right) and base (bottom left). The canonical trabecular volumes are thresholded at the critical value determined by the permutation control of type 1 error rate and colored by significantly higher rBV/TV in each species, as specified by the color of the row and column. The volumes are within a translucent canonical mesh of cortical bone.

palmar aspect of the base in *H. sapiens* relative to all other species (Figure 6). *H. sapiens* and *G. gorilla* demonstrated a concentration of significantly higher rBV/TV in the disto-radial region of the medullary cavity relative to both species of *Pan*, though it is more evident in the *P. troglodytes* comparisons. *H. sapiens* also had significantly less rBV/TV at the proximal extreme of the Mc1 head and throughout the proximal half of the medullary cavity relative to all of the species. *G. gorilla* also showed this pattern relative to *P. paniscus*.

Mass-univariate Kruskal-Wallis tests of each Mc1 segment showed similar results to that of the whole Mc1 analysis. The *H. sapiens* Mc1 head demonstrated a significantly higher concentration in the radial aspect relative to other species (Figure 6). However, calculation of rBV/TV for this segment alone revealed a significantly higher ulno-palmar distribution in *G. gorilla* relative to *P. paniscus* and some significant differences between the *Pan* species in the deep structure of this segment that were not revealed within the Mc1 whole bone analysis.

As in the multivariate results, analysis of the medullary cavity in isolation revealed subtler interspecific differences that were previously obscured due to low amount of trabecular bone in this segment relative to head and base. *H. sapiens* had significantly lower rBV/TV in the

proximal region of the medullary cavity and higher rBV/TV than all other species in the disto-radial region; the latter difference was smallest relative to *Pongo* and more ulnarly-extended relative to both *Pan* species (Figure 7). *G. gorilla* also had significantly higher rBV/TV than both *Pan* species in this disto-radial region and significantly higher rBV/TV than *Pongo* in the radial medullary cavity. *Pongo* also had significantly more rBV/TV in the distal region, and significantly less rBV/TV in the proximal region, of the medullary cavity relative to both *Pan* species.

In the Mc1 base, *H. sapiens* had significantly higher rBV/TV in the radio-palmar aspect of the sub-articular surface and significantly lower rBV/TV in the disto-dorsal region relative to all other species. *G. gorilla* had significantly lower rBV/TV in the disto-dorsal region of the base relative to both *Pan* species, but significantly higher rBV/TV than *Pan* in the ulno-palmar aspect of the sub-articular surface (Figure 7).

4 | DISCUSSION

The aim of the present study was to analyze the entire trabecular structure of the extant hominid Mc1, including the deeper structure

DUNMORE ET AL.

AMERICAN JOURNAL OF
BIOLOGICAL ANTHROPOLOGY
The Official Journal of the American Association of Biological Anthropologists

WILEY | 11

of the base, medullary cavity and head, to identify functional signals that could be used to infer fossil hominin thumb use in the future. We predicted that *H. sapiens* would have significantly lower BV/TV than in other extant hominids. We also predicted that previously identified subarticular concentrations of rBV/TV that statistically distinguished *H. sapiens* from other extant hominins (Dunmore, Bardo, et al., 2020) would extend deeper into the trabecular structure. Finally, we also predicted that *H. sapiens* would have significantly greater rBV/TV than other species in the region directly beneath the disto-radial flange of the Mc1, the internal aspect of the 'entheseal organ' (Benjamin & McGonagle, 2009), to dissipate muscular forces from a larger OP.

4.1 | Absolute trabecular bone volume fraction in the first metacarpal

We predicted that *H. sapiens* would have significantly lower BV/TV than in other extant hominids and our results support this prediction. The present analysis found significantly lower Mc1 BV/TV in *H. sapiens*, and significantly higher Mc1 BV/TV in *P. paniscus*, relative to all other extant hominids in our sample (Figure 2; Table 2). These interspecific Mc1 differences are consistent with those reported for sub-articular trabecular structure of the second to fifth metacarpal heads (Mc2-Mc5) on a similar sample (Dunmore et al., 2019). Tsegai et al. (2018) also found higher BV/TV in the whole Mc3 head in *P. troglodytes* relative to *H. sapiens*, though the difference was not significant. The fact that these interspecific differences hold for all three segments of the Mc1 despite variation in loading of the proximal and distal joints, as well as the diaphysis, suggests that variation in absolute BV/TV most likely partially reflects non-functional systemic interspecific differences.

Low BV/TV in the lower limb of recent agriculturalist *H. sapiens* is thought to reflect decreased loading due to sedentism relative to more mobile Pleistocene and Holocene foraging populations (Chirchir et al., 2015; DeMars et al., 2021; Ryan & Shaw, 2015). Domesticated canids and captive felids also show lower BV/TV than their wild counterparts, but there does not appear to be a direct or simple relationship between home range size (a proxy for mobility) and BV/TV in the wild counterparts of these groups (Chirchir, 2021; Chirchir et al., 2022). Further, a potentially systemic pattern of reduced BV/TV in more distal elements of the lower limb appears to characterize both forager and agricultural *H. sapiens* populations, though the former group did possess higher BV/TV (Saers et al., 2016). Thus, while the trabecular gracility of the sedentary modern human lower limb may be principally related to lower activity, this relationship may be more complicated in other anatomical elements. Low upper limb BV/TV in recent *H. sapiens*, relative to Pleistocene *H. sapiens*, may also be attributed to an increased reliance on technology decreasing load on the arm and hand in sedentary populations (Chirchir et al., 2015; Ryan & Shaw, 2015). However, the fact that recent *H. sapiens* have lower BV/TV than *P. troglodytes* at many anatomical sites suggests that at least part of this difference is systemic (Tsegai et al., 2018), perhaps due to a pleiotropic effect of reducing loading of the lower limb, or

related to the changes in disease prevalence and nutrition associated with the transition to sedentism in the Holocene, or "self-domestication," or all of these factors as well as others (Chirchir, 2021; Chirchir et al., 2015).

The present Mc1 results support the idea that a reduction in sedentary modern human BV/TV is not solely a functional signal. The *H. sapiens* thumb is robust relative to other hominids (Bowland et al., 2021; Marzke, 2013; Morley et al., 2022; Niewoehner, 2001) and its thenar musculature, particularly the OP, is both physiologically larger and creates more torque than in *P. troglodytes* due to advantageous moment arms (Karakostis et al., 2021; Maki & Trinkaus, 2011; Marzke et al., 1999). Therefore, as the modern human thumb is likely more strongly loaded than in non-human hominids, we might expect the *H. sapiens* Mc1 to have significantly higher BV/TV than that of other hominids if the amount of trabecular bone is related solely to functional loads. Thus, the significantly lower BV/TV in recent *H. sapiens* found here is argued to partially reflect a systemic signal, as suggested by Chirchir et al. (2015). Furthermore, experimental studies of zoo-housed *P. paniscus* have shown that the thumb incurs minimal loading during arboreal locomotion (Samuel et al., 2018) and this species is not thought use its thumb more frequently or forcefully in manipulation than recent *H. sapiens*, *P. troglodytes*, or *G. gorilla* (Bardo et al., 2016, 2017). Therefore, significantly higher BV/TV in *P. paniscus* also does not match functional expectations and may be partly systemic. If these differences in absolute BV/TV are systemic, it is as yet unknown why *P. paniscus* may have systemically higher BV/TV than *P. troglodytes* and other extant hominids. It is, however, important to note that systemic trabecular patterns may still have functional signals superimposed upon them, as has been shown for differing segments of the *H. sapiens* lower limb (Saers et al., 2016).

4.2 | Functional signals within the deeper first metacarpal trabecular network

We predicted that previously identified interspecific differences in subarticular distributions of trabecular bone (Dunmore, Bardo, et al., 2020; Dunmore, Skinner, et al., 2020) would extend deeper into the trabecular network as it functions to carry loads to the diaphysis (Currey, 2002; Martin et al., 2015b; Zhou et al., 2014) and the results partially support our predictions. The univariate and multivariate results of the current study generally support those found at the subarticular surfaces of a similar Mc1 sample, which is perhaps not surprising (Dunmore, Bardo, et al., 2020; Dunmore, Skinner, et al., 2020; Figures 4–7; Table 3). However, here we show for the first time how relative trabecular distribution might vary throughout the epiphyses, and not just directly beneath the facets. Analysis of the deeper Mc1 trabecular volume demonstrates the subarticular concentrations of rBV/TV in the ulnar Mc1 head of *Pan* and *Pongo*, as well as in the radio-palmar Mc1 base in *H. sapiens*, did extend further into the trabecular structure as predicted. The ulno-palmar concentrations in the Mc1 head and base of *G. gorilla*, as well as the radial concentration in the *H. sapiens* Mc1 head, do not extend deeper into the trabecular

structure against our prediction. Nevertheless, this volumetric analysis of trabecular structure provides a clearer separation of *H. sapiens* from other hominids than previous sub-articular studies (Dunmore, Bardo, et al., 2020; Dunmore, Skinner, et al., 2020; Figures 4 and 5).

The significantly higher rBV/TV in the radial aspect of the *H. sapiens* Mc1 head and radio-palmar aspect of the proximal base relative to all other hominids is consistent with the joint posture of the Mc1 during thumb opposition to the fingers (D'Agostino et al., 2017; Dunmore, Skinner, et al., 2020). These subarticular patterns extend distally in the radio-palmar aspect of the Mc1 base, but do not extend into the deeper trabecular structure of the Mc1 head in *H. sapiens* (Figures 4, 5, and 7). This difference in trabecular distribution may be the result of the greater forces experienced by the trapezio-metacarpal joint relative to the metacarpophalangeal joint during human manipulation (Cooney 3rd & Chao, 1977; Rolian et al., 2011).

Our multivariate results also reveal that the ulnar concentration of subarticular rBV/TV in the Mc1 head of non-human hominids found by Dunmore, Bardo, et al. (2020) and Dunmore, Skinner, et al., (2020) was the edge of a deeper concentration that spreads across all but the radial aspect of this region (Figures 4 and 5). This pattern is consistent with frequent adduction of the metacarpophalangeal joint, which is the required posture of pad-to-side grips that are frequently used by non-human hominids (Bardo et al., 2016, 2017; Dunmore, Bardo, et al., 2020; Neufuss et al., 2019). As this volumetric rBV/TV concentration is not as spatially restricted as that found in *H. sapiens*, and thus not highlighted by the univariate results (Figure 6), this signal likely also reflects more varied loading of the distal thumb joint in non-human hominids. However, *G. gorilla* did show significantly higher rBV/TV in spatially restricted concentrations at the ulno-palmar aspect of the subarticular Mc1 head relative to *P. paniscus* and relative to both *Pan* species in the ulno-palmar aspect of the subarticular Mc1 base (Figure 7). This difference in distribution is consistent with greater or more habitual loading of the thumb in an adducted posture in *Gorilla* relative to *Pan*. The stresses at the trapeziometacapal joint, just below the Mc1 base have been modeled as highly intraspecifically variable in *P. paniscus* suggesting it habitually loads this joint in a variety of positions (van Leeuwen et al., 2021), consistent with absence of a defined trabecular concentration in the Mc1 base (Figures 3–5). The *Gorilla* Mc1 is also radio-ulnarly wider and more robust than *Pan* (Bowland et al., 2021; Galletta et al., 2019) suggesting it is more heavily used. Beyond the pad to side manipulative and power grips observed in both genera (Bardo et al., 2016, 2017; Marzke et al., 2015; Neufuss et al., 2019; Neufuss, Robbins, et al., 2017) *Gorilla* has been observed adducting their thumb during frequent interdigital brace and thumb-wrap grasps (Bardo et al., 2017; Neufuss et al., 2019). *Gorilla* has also been shown to adduct the thumb more often than *Pan* when power grasping very large substrates during locomotion (Neufuss, Robbins, et al., 2017). Thus, while data is sparse on the actual force non-human hominid thumbs experience during manipulation or locomotion (Marzke et al., 2015; Samuel et al., 2018), the present results are consistent with observed adducted thumb use in *Gorilla*. A similar signal in a fossil hominin Mc1 would be consistent with a thumb loaded in adduction.

4.3 | Trabecular structure beneath the first metacarpal disto-radial flange

H. sapiens among our sample was distinct in having a significantly higher trabecular concentration in the disto-radial aspect of the medullary cavity, as predicted (Figures 3, 5b, 7, and 8). This region of the medullary cavity lies directly beneath the disto-radial flange which is thought to provide a greater surface area for the insertion of the *m. opponens pollicis* (OP) tendon (Karakostis et al., 2021; Niewoehner, 2006; Trinkaus, 2016). This muscle can produce more torque in *H. sapiens* than in *Pan* due to its significantly larger physiological cross-sectional area and advantageous moment arms, partially created by the disto-radial ridge (Karakostis et al., 2021; Maki & Trinkaus, 2011; Marzke et al., 1999). Further while the OP acts to flex and secondarily adduct the thumb in *P. troglodytes*, it secondarily abducts the thumb in *H. sapiens* (Marzke et al., 1999), a movement necessary for forceful thumb opposition in pad-to-pad grips habitually used by *H. sapiens* during manipulation (Marzke, 1997, 2013; Marzke & Wullstein, 1996). Despite intraspecific variation in the actual insertion site of the OP (Jacofsky, 2009; Trinkaus, 2016), this trabecular bone concentration in *H. sapiens* likely helps resist the forces generated by a large OP during thumb opposition, by transferring tensile loads from the disto-radial flange to the more proximal cortical diaphysis, as part of the OP 'entheseal organ' (Benjamin & McGonagle, 2009). This interpretation is supported by the apparently highly-organized proximo-distal orientation of trabeculae in this region (Figure 8), but further quantitative analysis of trabecular orientation is required. The disto-radial medullary concentration of trabecular bone in *H. sapiens* is also consistent with the radial and radio-palmar signals found in the Mc1 head and base, respectively. These concentrations are all consistent with a habitually, forcefully opposed thumb in *H. sapiens* and finding all three in a fossil hominin Mc1 would provide further evidence for this thumb movement in that individual.

While *G. gorilla* has significantly less trabecular bone in the region beneath the disto-radial flange than in *H. sapiens*, it has significantly more than in both *Pan* species (Figure 7). This trabecular concentration extends further proximally in *G. gorilla* than in *H. sapiens* (Figures 3, 5, and 7). This is perhaps unsurprising given the radio-ulnar width, robust nature and disto-radial flange development of the *G. gorilla* Mc1 (Bowland et al., 2021; Hamrick & Inouye, 1995; Morley et al., 2022; Figure 8), but it initially appears at odds with ulno-palmar subarticular concentrations in the *G. gorilla* Mc1 head and base relative to *Pan*, discussed above. It may be that *G. gorilla* Mc1 trabecular structure is principally a response to a habitually adducted thumb and secondarily to a frequently abducted thumb. While *G. gorilla* has yet to be observed performing forceful thumb opposition (Bardo et al., 2017; Christel, 1993; Neufuss et al., 2019) studies have stressed the variety of thumb postures used by *Gorilla beringei* during complex manipulation (Byrne et al., 2001; Neufuss et al., 2019). Conversely it may be that, as in *P. troglodytes* (Marzke et al., 1999), the OP in *G. gorilla* secondarily adducts the thumb during flexion. If this is the case, the trabecular concentration found beneath the disto-radial flange in *G. gorilla* is consistent with thumb adduction signals found in
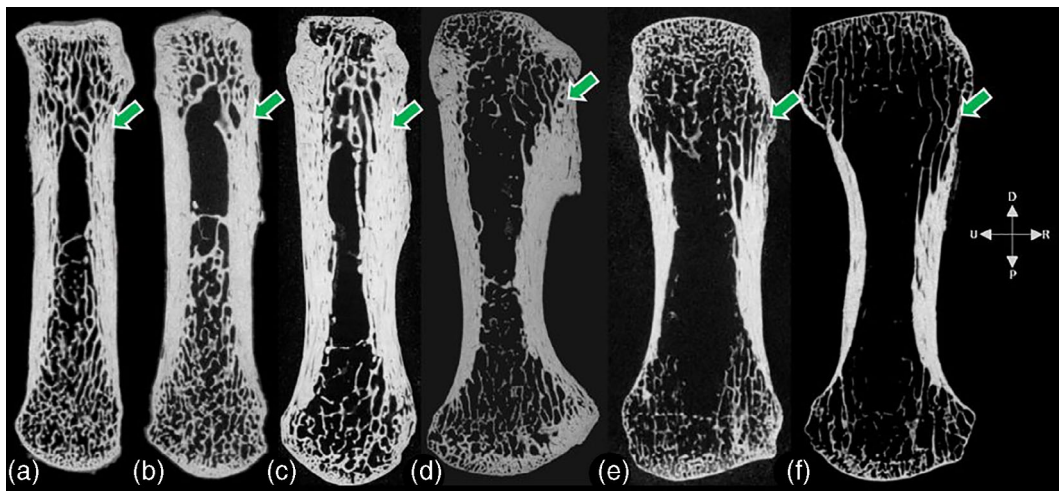
FIGURE 8 Coronal cross-sections of individuals representative of species at the extremes and centre of Pc1 in Figure 3. Images not to scale to aid in comparison of trabecular distributions. Note the large amount of trabecular bone, that extends into the proximal medullary cavity in the two *Pan paniscus* individuals (a,b: MRAC 29044 and 29052) and somewhat in the two *G. gorilla* individuals (c,d: MER 856 [flipped from left] and MER 264). The concentrations of trabecular bone beneath the disto-radial flange (approximately located at and below the green arrows) in the shaft of the gorillas are more strongly expressed than in the two *Pan* specimens but less so than in the *H. sapiens* (e,f: UNIFL 4865 and NHMW K5 2). These individuals have a trabecular concentration in the radial head and base (e,f). Note also the very low amount of trabecular bone in some humans (f). D, distal; P, proximal; R, radial; U, ulnar

the Mc1 head and base, as well as the observed thumb use (Bardo et al., 2017; Neufuss et al., 2019).

4.4 | The extent of the first metacarpal trabecular network

Although differences in the extent of the Mc1 trabecular bone network between *H. sapiens* and *Pan* have been qualitatively demonstrated previously (Skinner et al., 2015a; Stephens et al., 2016) this morphology has not been discussed or quantified across extant hominids. Here, a dense network of trabecular bone was found throughout the proximal medullary cavity of non-human hominids, especially in *P. paniscus* (Figures 3–7). It is worth noting that this medullary trabeculae does not drive significantly higher absolute BV/TV in *P. paniscus* as this difference is present in the other segments as well (Figure 2).

Medullary trabeculae are common in female birds, providing a calcium store for the production of egg shells (Alfonso-Carrillo et al., 2021; Taylor & Moore, 1953), but are relatively rare in other animals (Currey, 2002) as they are resorbed during growth (Martin et al., 2015b, p. 79) or during the healing of cortical bone (Martinez-Zelaya et al., 2021). A minor biomechanical role has been suggested for medullary trabeculae in large animals such as horses, providing support to bone marrow in large medullary cavities (Currey, 2002, p. 170). In specific groups of mammals however, long bone medullary trabeculae likely respond habitual loads in a similar manner as epiphyseal trabeculae (Ruff et al., 2006). In xentharans for example, the humerus and femur are often strongly elliptical in cross-section, making them appear more similar to flat bones with dense medullary trabecular networks that can extend from the epiphyseal trabecular structure (Montañez-Rivera et al., 2018; Straehl et al., 2013). In this morphology, it is probable that the medullary trabeculae are providing mechanical support between close cortical walls of the diaphysis (Currey, 2002, p. 219, Currey, 2012). The medullary trabeculae in the Mc1 of non-human hominids may well also be functional, as they appear principally as an extension of the proximal epiphyseal trabecular structure (Figures 3, 6, and 8). Epiphyseal trabecular bone acts to transmit load from the overlying joint to deeper trabecular structure and ultimately the diaphyseal cortical structure of long bones (Currey, 2002; Martin et al., 2015a; Zhou et al., 2014). Thus, medullary extension of this proximal network in non-human hominids would receive loads from, and presumably functionally adapt in the same manner as, Mc1 epiphyseal trabeculae.

If, as is argued from first principles here, these non-human hominid Mc1 medullary trabeculae are functional, their proximal rather than distal location in the cavity makes intuitive sense due to the higher forces thought to act on the trapeziometacarpal joint during manipulation (Cooney 3rd & Chao, 1977; Rolian et al., 2011). Distal extension of the proximal trabecular network would distribute forces more evenly over the diaphyseal cortical bone and provide greater elasticity to the diaphysis, than cortical bone alone (Currey, 2002). This may be a plastic response to manipulative or locomotor loading in the relatively small thumbs of non-human hominids (Almécija, Smaers, & Jungers, 2015).

Given the high external and muscular forces incurred by the modern *H. sapiens* Mc1 (Cooney & Chao, 1977; Rolian et al., 2011), it is surprising that *H. sapiens* do not also show a distal extension of trabeculae within the medullary cavity. However, the distinct absence of medullary trabeculae in humans may be due to the concentrated trabecular distribution in regions of habitual loading

14 | WILEY— AMERICAN JOURNAL OF **BIOLOGICAL ANTHROPOLOGY** The Official Journal of the American Association of Biological Anthropologists

DUNMORE ET AL.

(D'Agostino et al., 2017; Dunmore, Bardo, et al., 2020; Figures 3–6), robust external shape and cortical structure (Bowland et al., 2021; Dunmore, Skinner, et al., 2020; Galletta et al., 2019; Marchi et al., 2017; Marzke et al., 2010; Morley et al., 2022; Wong et al., 2018; Figure S7), as well as other soft tissue adaptations for manipulation (Marzke, 2013; van Leeuwen et al., 2018). That is, other *H. sapiens* Mc1 morphology may make medullary trabeculae unnecessary for the efficient resistance of incurred loads. It is also intuitive to argue this may be due to the, arguably systemic, lower BV/TV in humans relative to other hominids. While this factor may play a role in a lack of *H. sapiens* medullary trabeculae, *Gorilla* has a higher BV/TV throughout the Mc1 than humans and also has this pattern of less medullary trabeculae, at least relative to other non-human extant hominid species. Like *H. sapiens*, the externally robust Mc1 of *G. gorilla* (Bowland et al., 2021; Hamrick & Inouye, 1995) has significantly more spatially concentrated subarticular trabecular bone in the Mc1 head and base, as well as less trabeculae in proximal portion of the medullary cavity than that of both *Pan* species (Figures 6 and 7). The fact that *Gorilla* Mc1 external morphology and distal extension of trabecular network can be described as intermediate between *Homo* and *Pan* adds credence to this biomechanical interpretation of medullary trabeculae. However, more work on medullary trabeculae is needed to understand their function. In any case, there does appear to be a morphological polarity in extension of trabeculae into the medullary cavity, between extant non-human hominids and *H. sapiens*, which will aid functional inference of fossil hominin Mc1 material.

4.5 | Limitations

There are some limitations to this study that should be acknowledged. The human sample was restricted to right-sided Mc1s whereas the non-human hominid samples were taken from left and right hands. While this was done to mitigate any potential effect of cross-population right handedness in humans (Faurie et al., 2005), which is not found in other living hominids (Cashmore et al., 2008; Papademetriou et al., 2005), it may be argued that this approach biases the distribution patterns of trabecular bone volume. Trabecular bone volume fraction is higher in the right Mc1 of modern humans compared with the left (Stephens et al., 2016). However, the contra-lateral Mc1s of each non-human hominid studied here, did not show clear differences in rBV/TV distribution (Figure S5).

Our study also found that *Pongo* had the highest degree of variability among our sample (Figures 4 and 5b) and fewest number of significant differences with other taxa (Table 3, Figures 6 and 7) making functional interpretations difficult beyond their generally non-human hominid-like pattern. High variation in *Pongo* may be the result of the conflation of several *Pongo* sub-species, each with a potentially different pattern of rBV/TV distribution. These species were amalgamated due to the difficulty in obtaining high-resolution CT scans of complete adult non-pathological *Pongo* Mc1s, which also resulted in a lower sample size for this group than others ($n = 7$). This low sample size reduced statistical power in the mass-univariate analysis and

therefore may also have been a factor in the relative lack of differences between *Pongo* and other species. Future analysis of a larger *Pongo* sample would ameliorate these issues.

5 | CONCLUSION

This analysis found significantly higher absolute trabecular volume throughout the first metacarpal of *P. paniscus* and significantly lower absolute trabecular volume in *H. sapiens* relative to all other living hominids, which are interspecific patterns that most likely reflect systemic factors. The results generally supported the previously reported sub-articular interspecific differences in trabecular bone distribution, consistent with observed thumb use, and delimited their extension into the deeper trabecular structure. Trabecular concentrations beneath both Mc1 joints that were radial in *H. sapiens* and ulnar in *G. gorilla*, did not extend into the deeper trabecular network. Deeper trabecular concentrations were consistent with more varied use of a primarily adducted distal thumb joint in *Pan* and *Pongo*, as well as a more heavily loaded proximal Mc1 joint in *H. sapiens*. We also quantified variation in the distal extension of the proximal trabecular network into the medullary cavity in non-human hominids and the presence of a trabecular concentration beneath the disto-radial flange in *H. sapiens*, and to a lesser extent *Gorilla*. These suites of trabecular signals reflect observed hand use in living hominids and will help future research infer thumb use, as well as manipulative and thus technological capabilities, in fossil hominins. In particular, co-occurring concentrations of trabecular bone in the radial aspects of a fossil Mc1 head, base and beneath the disto-radial flange, appear to evidence a thumb habitually loaded in opposition to the fingers.

AUTHOR CONTRIBUTIONS
Christopher J. Dunmore: Conceptualization (lead); data curation (equal); formal analysis (lead); methodology (lead); software (equal); visualization (lead); writing – original draft (lead); writing – review and editing (lead). **Sebastian Bachmann:** Conceptualization (supporting); data curation (supporting); formal analysis (equal); methodology (equal); software (lead); validation (supporting); writing – review and editing (supporting). **Alexander Synek:** Conceptualization (supporting); formal analysis (supporting); methodology (supporting); software (equal); writing – review and editing (supporting). **Dieter Pahr:** Conceptualization (supporting); formal analysis (supporting); methodology (supporting); software (supporting); writing – review and editing (supporting). **Matthew M. Skinner:** Conceptualization (supporting); data curation (equal); funding acquisition (lead); writing – original draft (supporting); writing – review and editing (supporting). **Tracy Kivell:** Conceptualization (supporting); writing – original draft (supporting); writing – review and editing (supporting).

DUNMORE ET AL.

AMERICAN JOURNAL OF
BIOLOGICAL ANTHROPOLOGY
The Official Journal of the American Association of Biological Anthropologists

WILEY 15

DATA AVAILABILITY STATEMENT

Access to these computed tomography (CT) scans curated at the University of Kent is available via the relevant curatorial institution. The data that support the findings of this study are available from the corresponding author upon reasonable request.

ORCID

Christopher J. Dunmore 🅳 https://orcid.org/0000-0002-8634-9777
Sebastian Bachmann 🅳 https://orcid.org/0000-0002-6533-3602
Tracy L. Kivell 🅳 https://orcid.org/0000-0001-5087-0897

REFERENCES

Alba, D. M., Moyà-Solà, S., & Köhler, M. (2003). Morphological affinities of the Australopithecus afarensis hand on the basis of manual proportions and relative thumb length. *Journal of Human Evolution*, 44(2), 225–254. https://doi.org/10.1016/S0047-2484(02)00207-5

Alfonso-Carrillo, C., Benavides-Reyes, C., de los Mozos, J., Dominguez-Gasca, N., Sanchez-Rodríguez, E., Garcia-Ruiz, A. I., & Rodriguez-Navarro, A. B. (2021). Relationship between bone quality, egg production and eggshell quality in laying hens at the end of an extended production cycle (105 weeks). *Animals*, 11(3), 623. https://doi.org/10.3390/ani11030623

Almécija, S., Smaers, J. B., & Jungers, W. L. (2015). The evolution of human and ape hand proportions. *Nature Communications*, 6(1), 7717. https://doi.org/10.1038/ncomms8717

Almécija, S., Wallace, I. J., Judex, S., Alba, D. M., & Moyà-Solà, S. (2015). Comment on "human-like hand use in *Australopithecus africanus*.". *Science*, 348(6239), 1101. https://doi.org/10.1126/science.aaa8414

Anderson, M. J., & Walsh, D. C. I. (2013). Permanova, anosim, and the mantel test in the face of heterogeneous dispersions: What null hypothesis are you testing? *Ecological Monographs*, 83(4), 557–574. https://doi.org/10.1890/12-2010.1

Bachmann, S., Dunmore, C. J., Skinner, M. M., Pahr, D. H., & Synek, A. (2022). A computational framework for canonical holistic morphometric analysis of trabecular bone. *Scientific Reports*, 12(1), 5187. https://doi.org/10.1038/s41598-022-09063-6

Barak, M. M., Lieberman, D. E., & Hublin, J.-J. (2011). A Wolff in sheep's clothing: Trabecular bone adaptation in response to changes in joint loading orientation. *Bone*, 49(6), 1141–1151. https://doi.org/10.1016/j.bone.2011.08.020

Barak, M. M., Lieberman, D. E., & Hublin, J.-J. (2013). Of mice, rats and men: Trabecular bone architecture in mammals scales to body mass with negative allometry. *Journal of Structural Biology*, 183(2), 123–131. https://doi.org/10.1016/j.jsb.2013.04.009

Bardo, A., Borel, A., Meunier, H., Guéry, J.-P., & Pouydebat, E. (2016). Behavioral and functional strategies during tool use tasks in bonobos. *American Journal of Physical Anthropology*, 161(1), 125–140. https://doi.org/10.1002/ajpa.23015

Bardo, A., Cornette, R., Borel, A., & Pouydebat, E. (2017). Manual function and performance in humans, gorillas, and orangutans during the same tool use task. *American Journal of Physical Anthropology*, 164(4), 821–836. https://doi.org/10.1002/ajpa.23323

Barmakian, J. T. (1992). Anatomy of the joints of the thumb. *Hand Clinics*, 8(4), 683–691. https://doi.org/10.1016/S0749-0712(21)00735-6

Benjamin, M., & McGonagle, D. (2009). The enthesis organ concept and its relevance to the spondyloarthropathies. In C. López-Larrea & R. Díaz-Peña (Eds.), *Molecular mechanisms of spondyloarthropathies* (pp. 57–70). Springer. https://doi.org/10.1007/978-1-4419-0298-6_4

Bird, E. E., Kivell, T. L., & Skinner, M. M. (2021). Cortical and trabecular bone structure of the hominoid capitate. *Journal of Anatomy*, 239(2), 351–373. https://doi.org/10.1111/joa.13437

Bowland, L. A., Scott, J. E., Kivell, T. L., Patel, B. A., Tocheri, M. W., & Orr, C. M. (2021). Homo Naledi pollical metacarpal shaft morphology is distinctive and intermediate between that of australopiths and other members of the genus homo. *Journal of Human Evolution*, 158, 103048. https://doi.org/10.1016/j.jhevol.2021.103048

Bucchi, A., Luengo, J., Manzanares-Céspedes, M. C., Bucchi, C., & Lorenzo, C. (2020). Relation between muscle architecture and first metacarpal morphology, and its implications for human hand evolution. *Homo*, 101–109, 101–109. https://doi.org/10.1127/homo/2020/1149

Byrne, R. W., Corp, N., & Byrne, J. M. (2001). Manual dexterity in the gorilla: Bimanual and digit role differentiation in a natural task. *Animal Cognition*, 4(3–4), 347–361. https://doi.org/10.1007/s100710100083

Cashmore, L., Uomini, N., & Chapelain, A. (2008). The evolution of handedness in humans and great apes: A review and current issues. *Journal of Anthropological Sciences*, 86, 7–35.

Chirchir, H. (2021). Trabecular bone in domestic dogs and wolves: Implications for understanding human self-domestication. *The Anatomical Record*, 304(1), 31–41. https://doi.org/10.1002/ar.24510

Chirchir, H., Kivell, T. L., Ruff, C. B., Hublin, J.-J., Carlson, K. J., Zipfel, B., & Richmond, B. G. (2015). Recent origin of low trabecular bone density in modern humans. *Proceedings of the National Academy of Sciences*, 112(2), 366–371. https://doi.org/10.1073/pnas.1411696112

Chirchir, H., Ruff, C., Helgen, K. M., & Potts, R. (2022). Effects of reduced mobility on trabecular bone density in captive big cats. *Royal Society Open Science*, 9(3), 211345. https://doi.org/10.1098/rsos.211345

Christel, M. (1993). Grasping techniques and hand preferences in Hominoidea. In H. Preuschoft & D. J. Chivers (Eds.), *Hands of primates* (pp. 91–108). Springer. https://doi.org/10.1007/978-3-7091-6914-8_7

Cooney, W., 3rd, & Chao, E. Y. (1977). Biomechanical analysis of static forces in the thumb during hand function. *JBJS*, 59(1), 27–36.

Currey, J. D. (2002). *Bones: Structure and mechanics*. Princeton University Press.

Currey, J. D. (2012). The structure and mechanics of bone. *Journal of Materials Science*, 47(1), 41–54. https://doi.org/10.1007/s10853-011-5914-9

D'Agostino, P., Dourthe, B., Kerkhof, F., Harry Van Lenthe, G., Stockmans, F., & Vereecke, E. E. (2017). In vivo biomechanical behavior of the trapeziometacarpal joint in healthy and osteoarthritic subjects. *Clinical Biomechanics*, 49, 119–127. https://doi.org/10.1016/j.clinbiomech.2017.09.006

16 | WILEY—**AMERICAN JOURNAL OF BIOLOGICAL ANTHROPOLOGY** *The Official Journal of the American Association of Biological Anthropologists*

DUNMORE ET AL.

Deckers, K., Tsegai, Z. J., Skinner, M. M., Zeininger, A., & Kivell, T. L. (2022). Ontogenetic changes to metacarpal trabecular bone structure in mountain and western lowland gorillas. *Journal of Anatomy*, 241(1), 82–100. https://doi.org/10.1111/joa.13630

DeMars, L. J. D., Stephens, N. B., Saers, J. P. P., Gordon, A., Stock, J. T., & Ryan, T. M. (2021). Using point clouds to investigate the relationship between trabecular bone phenotype and behavior: An example utilizing the human calcaneus. *American Journal of Human Biology*, 33(2), e23468. https://doi.org/10.1002/ajhb.23468

Doershuk, L. J., Saers, J. P. P., Shaw, C. N., Jashashvili, T., Carlson, K. J., Stock, J. T., & Ryan, T. M. (2019). Complex variation of trabecular bone structure in the proximal humerus and femur of five modern human populations. *American Journal of Physical Anthropology*, 168(1), 104–118. https://doi.org/10.1002/ajpa.23725

Doube, M., Kłosowski, M. M., Arganda-Carreras, I., Cordelières, F. P., Dougherty, R. P., Jackson, J. S., Schmid, B., Hutchinson, J. R., & Shefelbine, S. J. (2010). BoneJ: Free and extensible bone image analysis in ImageJ. *Bone*, 47(6), 1076–1079. https://doi.org/10.1016/j.bone.2010.08.023

Doube, M., Kłosowski, M. M., Wiktorowicz-Conroy, A. M., Hutchinson, J. R., & Shefelbine, S. J. (2011). Trabecular bone scales allometrically in mammals and birds. *Proceedings of the Royal Society B: Biological Sciences*, 278(1721), 3067–3073. https://doi.org/10.1098/rspb.2011.0069

Dunmore, C. J., Bardo, A., Skinner, M. M., & Kivell, T. L. (2020). Trabecular variation in the first metacarpal and manipulation in hominids. *American Journal of Physical Anthropology*, 171(2), 219–241. https://doi.org/10.1002/ajpa.23974

Dunmore, C. J., Kivell, T. L., Bardo, A., & Skinner, M. M. (2019). Metacarpal trabecular bone varies with distinct hand-positions used in hominid locomotion. *Journal of Anatomy*, 235(1), 45–66. https://doi.org/10.1111/joa.12966

Dunmore, C. J., Skinner, M. M., Bardo, A., Berger, L. R., Hublin, J.-J., Pahr, D. H., Rosas, A., Stephens, N. B., & Kivell, T. L. (2020). The position of Australopithecus sediba within fossil hominin hand use diversity. *Nature Ecology & Evolution*, 4(7), 911–918. https://doi.org/10.1038/s41559-020-1207-5

Dunmore, C. J., Wollny, G., & Skinner, M. M. (2018). MIA-clustering: A novel method for segmentation of paleontological material. *PeerJ*, 6, e4374.

Faurie, C., Schiefenhövel, W., le Bomin, S., Billiard, S., & Raymond, M. (2005). Variation in the frequency of left-handedness in traditional societies. *Current Anthropology*, 46(1), 142–147. https://doi.org/10.1086/427101

Friston, K. J., Holmes, A. P., Worsley, K. J., Poline, J.-P., Frith, C. D., & Frackowiak, R. S. J. (1994). Statistical parametric maps in functional imaging: A general linear approach. *Human Brain Mapping*, 2(4), 189–210. https://doi.org/10.1002/hbm.460020402

Galletta, L., Stephens, N. B., Bardo, A., Kivell, T. L., & Marchi, D. (2019). Three-dimensional geometric morphometric analysis of the first metacarpal distal articular surface in humans, great apes and fossil hominins. *Journal of Human Evolution*, 132, 119–136. https://doi.org/10.1016/j.jhevol.2019.04.008

Georgiou, L., Dunmore, C. J., Bardo, A., Buck, L. T., Hublin, J.-J., Pahr, D. H., Stratford, D., Synek, A., Kivell, T. L., & Skinner, M. M. (2020). Evidence for habitual climbing in a Pleistocene hominin in South Africa. *Proceedings of the National Academy of Sciences*, 117(15), 8416–8423. https://doi.org/10.1073/pnas.1914481117

Gross, T., Kivell, T. L., Skinner, M. M., Nguyen, H., & Pahr, D. H. (2014). Holistic analysis of bone. *Palaeontologia Electronica*, 17(3), 1. https://doi.org/10.26879/438

Grosskopf, B. (2015). *Der Vergessene Friedhof*. Universitätsverlag Göttingen. https://doi.org/10.17875/gup2015-884

Hamrick, M. W., & Inouye, S. E. (1995). Thumbs, tools, and early humans. *Science*, 268(5210), 586–587; author reply 589. https://doi.org/10.1126/science.7725112

Hildebrand, T., & Rüegsegger, P. (1997). A new method for the model-independent assessment of thickness in three-dimensional images.

Journal of Microscopy, 185(1), 67–75. https://doi.org/10.1046/j.1365-2818.1997.1340694.x

Jacofsky, M. C. (2009). Comparative muscle moment arms of the primate thumb: *Homo*, *Pan*, *Pongo*, and *Papio*, Ph.D. Thesis, Arizona State University, AZ, USA. https://www.proquest.com/docview/304832487/abstract/57C303B14F964FB7PQ/1

Karakostis, F. A., Haeufle, D., Anastopoulou, I., Moraitis, K., Hotz, G., Tourloukis, V., & Harvati, K. (2021). Biomechanics of the human thumb and the evolution of dexterity. *Current Biology*, 31(6), 1317–1325. https://doi.org/10.1016/j.cub.2020.12.041

Karakostis, F. A., Jeffery, N., & Harvati, K. (2019). Experimental proof that multivariate patterns among muscle attachments (entheses) can reflect repetitive muscle use. *Scientific Reports*, 9(1), 16577. https://doi.org/10.1038/s41598-019-53021-8

Karakostis, F. A., & Lorenzo, C. (2016). Morphometric patterns among the 3D surface areas of human hand entheses. *American Journal of Physical Anthropology*, 160(4), 694–707. https://doi.org/10.1002/ajpa.22999

Karakostis, F. A., Vlachodimitropoulos, D., Piagkou, M., Scherf, H., Harvati, K., & Moraitis, K. (2019). Is bone elevation in hand muscle attachments associated with biomechanical stress? A histological approach to an anthropological question. *The Anatomical Record*, 302(7), 1093–1103. https://doi.org/10.1002/ar.23984

Karakostis, F. A., Wallace, I. J., Konow, N., & Harvati, K. (2019). Experimental evidence that physical activity affects the multivariate associations among muscle attachments (entheses). *Journal of Experimental Biology*, 222(23), 1–7. https://doi.org/10.1242/jeb.213058

Key, A. J. M., & Dunmore, C. J. (2015). The evolution of the hominin thumb and the influence exerted by the non-dominant hand during stone tool production. *Journal of Human Evolution*, 78, 60–69. https://doi.org/10.1016/j.jhevol.2014.08.006

Key, A. J. M., Dunmore, C. J., & Marzke, M. W. (2019). The unexpected importance of the fifth digit during stone tool production. *Scientific Reports*, 9(1), 16724. https://doi.org/10.1038/s41598-019-53332-w

Kivell, T. L. (2016). A review of trabecular bone functional adaptation: What have we learned from trabecular analyses in extant hominoids and what can we apply to fossils? *Journal of Anatomy*, 228(4), 569–594. https://doi.org/10.1111/joa.12446

Kivell, T. L., Deane, A. S., Tocheri, M. W., Orr, C. M., Schmid, P., Hawks, J., Berger, L. R., & Churchill, S. E. (2015). The hand of homo Naledi. *Nature Communications*, 6(1), 8431. https://doi.org/10.1038/ncomms9431

Kivell, T. L., Kibii, J. M., Churchill, S. E., Schmid, P., & Berger, L. R. (2011). *Australopithecus sediba* hand demonstrates mosaic evolution of locomotor and manipulative abilities. *Science*, 333(6048), 1411–1417. https://doi.org/10.1126/science.1202625

Kivell, T. L., Lemelin, P., Richmond, B. G., & Schmitt, D. (2016). *The evolution of the primate hand: Anatomical, developmental, functional, and paleontological evidence*. Springer.

Lazar, N. A. (2008). Multiple testing in fMRI: The problem of "thresholding.". In *Statistics for biology and health. The statistical analysis of functional MRI data* (pp. 1–24). Springer. https://doi.org/10.1007/978-0-387-78191-4_10

Lovejoy, C. O., McCollum, M. A., Reno, P. L., & Rosenman, B. A. (2003). Developmental biology and human evolution. *Annual Review of Anthropology*, 32(1), 85–109. https://doi.org/10.1146/annurev.anthro.32.061002.093223

MacArthur, R. H. (1957). On the relative abundance of BIRD species. *Proceedings of the National Academy of Sciences of the United States of America*, 43(3), 293–295.

Maki, J., & Trinkaus, E. (2011). Opponens pollicis mechanical effectiveness in Neandertals and early modern humans. *PaleoAnthropology*, 2011, 62–71.

Marangoni, A., Belli, M., Caramelli, D., Moggi-Cecchi, J., Zavattaro, M., & Manzi, G. (2011). Tierra del Fuego, its ancient inhabitants, and the collections of skeletal remains in the museums of anthropology of Florence and Rome. https://www.semanticscholar.org/paper/Tierra-del-

DUNMORE ET AL.

AMERICAN JOURNAL OF BIOLOGICAL ANTHROPOLOGY
The Official Journal of the American Association of Biological Anthropologists

WILEY | 17

Fuego%2C-its-ancient-inhabitants%2C-and-the-Marangoni-Belli/98df91d8ec4a848b8de66a7094a2121bf032a8a5

Marchi, D., Proctor, D. J., Huston, E., Nicholas, C. L., & Fischer, F. (2017). Morphological correlates of the first metacarpal proximal articular surface with manipulative capabilities in apes, humans and south African early hominins. *Comptes Rendus Palevol*, 16(5), 645–654. https://doi.org/10.1016/j.crpv.2016.09.002

Martin, R. B., Burr, D. B., Sharkey, N. A., & Fyhrie, D. P. (2015a). Growth, modeling and remodeling of bone. In R. B. Martin, D. B. Burr, N. A. Sharkey, & D. P. Fyhrie (Eds.), *Skeletal tissue mechanics* (pp. 95–173). Springer. https://doi.org/10.1007/978-1-4939-3002-9_3

Martin, R. B., Burr, D. B., Sharkey, N. A., & Fyhrie, D. P. (2015b). Skeletal Biology. In R. B. Martin, D. B. Burr, N. A. Sharkey, & D. P. Fyhrie (Eds.), *Skeletal tissue mechanics* (pp. 35–93). Springer. https://doi.org/10.1007/978-1-4939-3002-9_2

Martinez-Zelaya, V. R., Archilha, N. L., Calasans-Maia, M., Farina, M., & Rossi, A. M. (2021). Trabecular architecture during the healing process of a tibial diaphysis defect. *Acta Biomaterialia*, 120, 181–193. https://doi.org/10.1016/j.actbio.2020.08.028

Marzke, M. W. (1997). Precision grips, hand morphology, and tools. *American Journal of Physical Anthropology*, 102(1), 91–110. https://doi.org/10.1002/(SICI)1096-8644(199701)102:1\textless91::AID-AJPA8\textgreater3.0.CO;2-G

Marzke, M. W. (2013). Tool making, hand morphology and fossil hominins. *Philosophical Transactions of the Royal Society, B: Biological Sciences*, 368(1630), 20120414. https://doi.org/10.1098/rstb.2012.0414

Marzke, M. W., Marchant, L. F., McGrew, W. C., & Reece, S. P. (2015). Grips and hand movements of chimpanzees during feeding in Mahale Mountains National Park, Tanzania. *American Journal of Physical Anthropology*, 156(3), 317–326. https://doi.org/10.1002/ajpa.22651

Marzke, M. W., Marzke, R. F., Linscheid, R. L., Smutz, P., Steinberg, B., Reece, S., & An, K. N. (1999). Chimpanzee thumb muscle cross sections, moment arms and potential torques, and comparisons with humans. *American Journal of Physical Anthropology*, 110(2), 163–178. https://doi.org/10.1002/(SICI)1096-8644(199910)110:2\textless163::AID-AJPA4\textgreater3.0.CO;2-A

Marzke, M. W., & Shackley, M. S. (1986). Hominid hand use in the pliocene and pleistocene: Evidence from experimental archaeology and comparative morphology. *Journal of Human Evolution*, 15(6), 439–460. https://doi.org/10.1016/S0047-2484(86)80027-6

Marzke, M. W., Tocheri, M. W., Steinberg, B., Femiani, J. D., Reece, S. P., Linscheid, R. L., Orr, C. M., & Marzke, R. F. (2010). Comparative 3D quantitative analyses of trapeziometacarpal joint surface curvatures among living catarrhines and fossil hominins. *American Journal of Physical Anthropology*, 141(1), 38–51. https://doi.org/10.1002/ajpa.21112

Marzke, M. W., Toth, N., Schick, K., Reece, S., Steinberg, B., Hunt, K., Linscheid, R. L., & An, K. N. (1998). EMG study of hand muscle recruitment during hard hammer percussion manufacture of Oldowan tools. *American Journal of Physical Anthropology*, 105(3), 315–332.

Marzke, M. W., & Wullstein, K. L. (1996). Chimpanzee and human grips: A new classification with a focus on evolutionary morphology. *International Journal of Primatology*, 17(1), 117–139. https://doi.org/10.1007/BF02696162

Montañez-Rivera, I., Nyakatura, J. A., & Amson, E. (2018). Bone cortical compactness in 'tree sloths' reflects convergent evolution. *Journal of Anatomy*, 233(5), 580–591. https://doi.org/10.1111/joa.12873

Morley, J., Bucchi, A., Lorenzo, C., & Püschel, T. A. (2022). Characterizing the body morphology of the first metacarpal in the Homininae using 3D geometric morphometrics. *American Journal of Biological Anthropology*, 177(4), 748–759. https://doi.org/10.1002/ajpa.24473

Napier, J. R. (1960). Studies of the hands of living primates. *Proceedings of the Zoological Society of London*, 134(4), 647–657. https://doi.org/10.1111/j.1469-7998.1960.tb05606.x

Napier, J. R. (1962). Fossil hand bones from Olduvai Gorge. *Nature*, 196(4853), 409–411. https://doi.org/10.1038/196409a0

Napier, J. R. (1993). In R. H. Tuttle (Ed.), *Hands*. Princeton University Press.

Neufuss, J., Humle, T., Cremaschi, A., & Kivell, T. L. (2017). Nut-cracking behaviour in wild-born, rehabilitated bonobos (*Pan paniscus*): A comprehensive study of hand-preference, hand grips and efficiency. *American Journal of Primatology*, 79(2), e22589. https://doi.org/10.1002/ajp.22589

Neufuss, J., Robbins, M. M., Baeumer, J., Humle, T., & Kivell, T. L. (2017). Comparison of hand use and forelimb posture during vertical climbing in mountain gorillas (gorilla beringei beringei) and chimpanzees (pan troglodytes). *American Journal of Physical Anthropology*, 164(4), 651–664. https://doi.org/10.1002/ajpa.23303

Neufuss, J., Robbins, M. M., Baeumer, J., Humle, T., & Kivell, T. L. (2019). Manual skills for food processing by mountain gorillas (gorilla beringei beringei) in Bwindi impenetrable National Park, Uganda. *Biological Journal of the Linnean Society*, 127(3), 543–562. https://doi.org/10.1093/biolinnean/bly071

Nichols, T., & Hayasaka, S. (2003). Controlling the familywise error rate in functional neuroimaging: A comparative review. *Statistical Methods in Medical Research*, 12(5), 419–446. https://doi.org/10.1191/0962280203sm341ra

Niewoehner, W. A. (2001). Behavioral inferences from the Skhul/Qafzeh early modern human hand remains. *Proceedings of the National Academy of Sciences*, 98(6), 2979–2984. https://doi.org/10.1073/pnas.041588898

Niewoehner, W. A. (2006). Neanderthal hands in their proper perspective. In J.-J. Hublin, K. Harvati, & T. Harrison (Eds.), *Neanderthals revisited: New approaches and perspectives* (pp. 157–190). Springer Netherlands. https://doi.org/10.1007/978-1-4020-5121-0_9

Pahr, D. H., & Zysset, P. K. (2009). From high-resolution CT data to finite element models: Development of an integrated modular framework. *Computer Methods in Biomechanics and Biomedical Engineering*, 12(1), 45–57. https://doi.org/10.1080/10255840802144105

Paoli, G., Tarli, S. M. B., Klír, P., Strouhal, E., Tofanelli, S., Del Santo Valli, M. T., & Pavelcová, B. (1993). Paleoserology of the Christian population at Sayala (lower Nubia): An evaluation of the reliability of the results. *American Journal of Physical Anthropology*, 92(3), 263–272. https://doi.org/10.1002/ajpa.1330920304

Papademetriou, E., Sheu, C.-F., & Michel, G. F. (2005). A meta-analysis of primate hand preferences, particularly for reaching. *Journal of Comparative Psychology*, 119(1), 33–48. https://doi.org/10.1037/0735-7036.119.1.33

Pontzer, H., Lieberman, D. E., Momin, E., Devlin, M. J., Polk, J. D., Hallgrímsson, B., & Cooper, D. M. L. (2006). Trabecular bone in the bird knee responds with high sensitivity to changes in load orientation. *Journal of Experimental Biology*, 209(1), 57–65. https://doi.org/10.1242/jeb.01971

Rafferty, K. F. (1990). The functional and phylogenetic significance of the carpometacarpal joint of the thumb in anthropoid primates.

Richmond, B. G., Roach, N. T., & Ostrofsky, K. R. (2016). Evolution of the early hominin hand. In T. L. Kivell, P. Lemelin, B. G. Richmond, & D. Schmitt (Eds.), *The evolution of the primate hand: Anatomical, developmental, functional, and paleontological evidence* (pp. 515–543). Springer. https://doi.org/10.1007/978-1-4939-3646-5_18

Rolian, C., Lieberman, D. E., & Zermeno, J. P. (2011). Hand biomechanics during simulated stone tool use. *Journal of Human Evolution*, 61(1), 26–41. https://doi.org/10.1016/j.jhevol.2011.01.008

Ruff, C., Holt, B., & Trinkaus, E. (2006). Who's afraid of the big bad Wolff?: "Wolff's law" and bone functional adaptation. *American Journal of Physical Anthropology*, 129(4), 484–498. https://doi.org/10.1002/ajpa.20371

Ryan, T. M., & Shaw, C. N. (2013). Trabecular bone microstructure scales allometrically in the primate humerus and femur. *Proceedings of the

18 | WILEY—**AMERICAN JOURNAL OF BIOLOGICAL ANTHROPOLOGY**
The Official Journal of the American Association of Biological Anthropologists

DUNMORE ET AL.

Royal Society B: Biological Sciences, *280*(1758), 20130172. https://doi.org/10.1098/rspb.2013.0172

Ryan, T. M., & Shaw, C. N. (2015). Gracility of the modern *Homo sapiens* skeleton is the result of decreased biomechanical loading. *Proceedings of the National Academy of Sciences*, *112*(2), 372–377. https://doi.org/10.1073/pnas.1418646112

Saers, J. P. P., Cazorla-Bak, Y., Shaw, C. N., Stock, J. T., & Ryan, T. M. (2016). Trabecular bone structural variation throughout the human lower limb. *Journal of Human Evolution*, *97*, 97–108. https://doi.org/10.1016/j.jhevol.2016.05.012

Samuel, D. S., Nauwelaerts, S., Stevens, J. M. G., & Kivell, T. L. (2018). Hand pressures during arboreal locomotion in captive bonobos (pan paniscus). *Journal of Experimental Biology*, *221*(8), 1-13. https://doi.org/10.1242/jeb.170910

Shrewsbury, M. M., Marzke, M. W., Linscheid, R. L., & Reece, S. P. (2003). Comparative morphology of the pollical distal phalanx. *American Journal of Physical Anthropology*, *121*(1), 30–47. https://doi.org/10.1002/ajpa.10192

Skinner, M. M., Stephens, N. B., Tsegai, Z. J., Foote, A. C., Nguyen, N. H., Gross, T., Pahr, D. H., Hublin, J.-J., & Kivell, T. L. (2015a). Human-like hand use in *Australopithecus africanus*. *Science*, *347*(6220), 395–399. https://doi.org/10.1126/science.1261735

Skinner, M. M., Stephens, N. B., Tsegai, Z. J., Foote, A. C., Nguyen, N. H., Gross, T., Pahr, D. H., Hublin, J.-J., & Kivell, T. L. (2015b). Response to Comment on "Human-like hand use in *Australopithecus africanus*.". *Science*, *348*(6239), 1101. https://doi.org/10.1126/science.aaa8931

Sorrentino, R., Stephens, N. B., Marchi, D., DeMars, L. J. D., Figus, C., Bortolini, E., Badino, F., JPP, S., Bettuzzi, M., Boschin, F., Capecchi, G., Feletti, F., Guarnieri, T., May, H., Morigi, M. P., Parr, W., Ricci, S., Ronchitelli, A., Stock, J. T., ... Benazzi, S. (2021). Unique foot posture in Neanderthals reflects their body mass and high mechanical stress. *Journal of Human Evolution*, *161*, 103093. https://doi.org/10.1016/j.jhevol.2021.103093

Stauber, M., Rapillard, L., van Lenthe, G. H., Zysset, P., & Müller, R. (2006). Importance of individual rods and plates in the assessment of bone quality and their contribution to bone stiffness. *Journal of Bone and Mineral Research*, *21*(4), 586–595. https://doi.org/10.1359/jbmr.060102

Stephens, N. B., Kivell, T. L., Gross, T., Pahr, D. H., Lazenby, R. A., Hublin, J.-J., Hershkovitz, I., & Skinner, M. M. (2016). Trabecular architecture in the thumb of *Pan* and *Homo*: Implications for investigating hand use, loading, and hand preference in the fossil record. *American Journal of Physical Anthropology*, *161*(4), 603–619. https://doi.org/10.1002/ajpa.23061

Stephens, N. B., Kivell, T. L., Pahr, D. H., Hublin, J.-J., & Skinner, M. M. (2018). Trabecular bone patterning across the human hand. *Journal of Human Evolution*, *123*, 1–23. https://doi.org/10.1016/j.jhevol.2018.05.004

Straehl, F. R., Scheyer, T. M., Forasiepi, A. M., MacPhee, R. D., & Sánchez-Villagra, M. R. (2013). Evolutionary patterns of bone histology and bone compactness in Xenarthran mammal Long bones. *PLoS One*, *8*(7), e69275. https://doi.org/10.1371/journal.pone.0069275

Strouhal, E., & Jungwirth, J. (1979). Paleogenetics of the late Roman-early byzantine cemeteries at Sayala, Egyptian Nubia. *Journal of Human Evolution*, *8*(7), 699–703. https://doi.org/10.1016/0047-2484(79)90071-X

Sukhdeo, S., Parsons, J., Niu, X. M., & Ryan, T. M. (2020). Trabecular bone structure in the distal femur of humans, apes, and baboons. *The Anatomical Record*, *303*(1), 129–149. https://doi.org/10.1002/ar.24050

Susman, R. L. (1979). Comparative and functional morphology of hominoid fingers. *American Journal of Physical Anthropology*, *50*(2), 215–236. https://doi.org/10.1002/ajpa.1330500211

Susman, R. L. (1994). Fossil evidence for early hominid tool use. *Science*, *265*(5178), 1570–1573. https://doi.org/10.1126/science.8079169

Taylor, T. G., & Moore, J. H. (1953). Avian medullary bone. *Nature*, *172*(4376), 504–505. https://doi.org/10.1038/172504a0

Tocheri, M. W., Orr, C. M., Jacofsky, M. C., & Marzke, M. W. (2008). The evolutionary history of the hominin hand since the last common ancestor of *Pan* and *Homo*. *Journal of Anatomy*, *212*(4), 544–562. https://doi.org/10.1111/j.1469-7580.2008.00865.x

Trinkaus, E. (2016). The evolution of the hand in Pleistocene homo. In T. L. Kivell, P. Lemelin, B. G. Richmond, & D. Schmitt (Eds.), *The evolution of the primate hand: Anatomical, developmental, functional, and paleontological evidence* (pp. 545–571). Springer. https://doi.org/10.1007/978-1-4939-3646-5_19

Trinkaus, E., & Long, J. C. (1990). Species attribution of the Swartkrans member 1 first metacarpals: SK 84 and SKX 5020. *American Journal of Physical Anthropology*, *83*(4), 419–424. https://doi.org/10.1002/ajpa.1330830403

Tsegai, Z. J., Kivell, T. L., Gross, T., Nguyen, N. H., Pahr, D. H., Smaers, J. B., & Skinner, M. M. (2013). Trabecular bone structure correlates with hand posture and use in hominoids. *PLoS One*, *8*(11), e78781. https://doi.org/10.1371/journal.pone.0078781

Tsegai, Z. J., Skinner, M. M., Pahr, D. H., Hublin, J.-J., & Kivell, T. L. (2018). Systemic patterns of trabecular bone across the human and chimpanzee skeleton. *Journal of Anatomy*, *232*(4), 641–656.

van Leeuwen, T., van Lenthe, G. H., Vereecke, E. E., & Schneider, M. T. (2021). Stress distribution in the bonobo (*Pan paniscus*) trapeziometacarpal joint during grasping. *PeerJ*, *9*, e12068. https://doi.org/10.7717/peerj.12068

van Leeuwen, T., Vanhoof, M. J. M., Kerkhof, F. D., Stevens, J. M. G., & Vereecke, E. E. (2018). Insights into the musculature of the bonobo hand. *Journal of Anatomy*, *233*(3), 328–340. https://doi.org/10.1111/joa.12841

Wallace, I. J., Demes, B., & Judex, S. (2017). Onotgenetic and genetic influences on bone's repsonsiveness to mechanical signals. In *Building bones: Bone formation and development in anthropology* (pp. 233–253). Cambridge University Press.

Williams-Hatala, E. M., Hatala, K. G., Hiles, S., & Rabey, K. N. (2016). Morphology of muscle attachment sites in the modern human hand does not reflect muscle architecture. *Scientific Reports*, *6*(1), 28353. https://doi.org/10.1038/srep28353

Wong, A. L., Meals, C. G., & Ruff, C. B. (2018). Computed tomographic analysis of the internal structure of the metacarpals and its implications for hand use, pathology, and surgical intervention. *Anatomical Science International*, *93*(2), 231–237. https://doi.org/10.1007/s12565-017-0400-3

Wood-Jones, F. (1917). *Arboreal man*. Creative Media Partners, LLC.

Wunderlich, R. E., & Jungers, W. L. (2009). Manual digital pressures during knuckle-walking in chimpanzees (pan troglodytes). *American Journal of Physical Anthropology*, *139*(3), 394–403. https://doi.org/10.1002/ajpa.20994

Zhou, G.-Q., Pang, Z.-H., Chen, Q.-Q., He, W., Chen, Z.-Q., Chen, L.-L., & Li, Z.-Q. (2014). Reconstruction of the biomechanical transfer path of femoral head necrosis: A subject-specific finite element investigation. *Computers in Biology and Medicine*, *52*, 96–101. https://doi.org/10.1016/j.compbiomed.2014.04.002

SUPPORTING INFORMATION

Additional supporting information can be found online in the Supporting Information section at the end of this article.